model. Therefore, we focused on the intracellular domain of Tie2 for dimerization in our next experiments.

We transfected Tie2-HAVN and Tie2/Tie1* chimeric genes fused with Myc-tagged VC155 into HEK293T cells. When the C-terminal of Tie2 (from 975 to 1088 amino acids) was replaced by the Tie1 sequence, BiFC was significantly attenuated (Fig. 4*B*). There are differences in 13 amino acids between Tie2 and Tie1 (Fig. 4*C*). Therefore, we mutated Tie2 where its sequence is different from Tie1 domain by domain and observed Tie2-Tie2/mutant dimerization. We found that a YIA sequence within Tie2 (975–977) is critical for dimerization (Fig. 4*D*). Next, we introduced point mutations into this YIA domain. We found that no single mutation was responsible for reducing Tie2 dimerization, but rather the whole YIA tandem sequence was involved (Fig. 4*E*). We generated mutant Tie2 (Tie2YIA/LAS) in which the YIA domain of Tie2 was replaced by LAS. Tie2-Tie2YIA/LAS and Tie2YIA/LAS-Tie2YIA/LAS dimerization was not significantly different, suggesting that both Tie2 YIA domains in the cytoplasmic region are required for dimerization (Fig. 4*F*). When phosphorylation of Tie2YIA/LAS was assessed, it was found that mere overexpression did not induce it (supplemental Fig. S4).

Tie2YIA/LAS Monomer Mutants Can Be Dimerized and Phosphorylated by Ligand Binding—Tie2 can form ligand-independent inactive dimers; it has therefore been suggested that receptor dimerization and activation are mechanistically distinct and separable events (19, 30). Next, we analyzed whether Angl binding to the inactive monomer mutant Tie2YIA/LAS induced dimerization and activation of Tie2. Phosphorylation of WT Tie2 by exogenous Angl did not increase the intensity of BiFC developed by either Tie2-Tie2 (Fig. 5*A*). On the contrary, Angl stimulation decreased BiFC intensity after 30 min. This suggests that internalization and degradation of Tie2 was induced after Tie2 phosphorylation (30). Interestingly, we found that Tie2YIA/LAS prominently enhanced BiFC intensity under Angl stimulation for 1 h (Fig. 5*B*). Microscopy showed that Tie2 formed ligand-independent dimers and was internalized upon Angl stimulation (Fig. 6*A*). In contrast, Tie2YIA/LAS dimerization was not detected in the absence of Angl. However, BiFC signals due to dimerization did occur upon stimulation with Angl, although to a lesser extent than in WT Tie2. This suggests that YIA mutations in Tie2 did not completely prevent Tie2 dimerization (Fig. 6*B*).

Finally, we investigated how the lack of Tie2 ligand-independent dimerization affected its phosphorylation and downstream Erk signaling. When the time course of Tie2 phosphorylation was recorded in the presence of a fixed dose of Angl (200 ng/ml), no significant differences between wild-type Tie2 and Tie2YIA/LAS were observed (Fig. 7*A*). However, when phosphorylation was measured after stimulation for 10 min with different doses of Angl, Tie2 and Erk phosphorylation by Tie2YIA/LAS decreased at a high dose (350~500 ng/ml) of Angl compared with wild-type Tie2 (Fig. 7, *B* and *C*). These findings suggest that the YIA domain of Tie2 is not indispensable for dimerization of Tie2 but is used for forming non-ligand-mediated dimerization of Tie2 to effectively react to a higher dose of Angl.

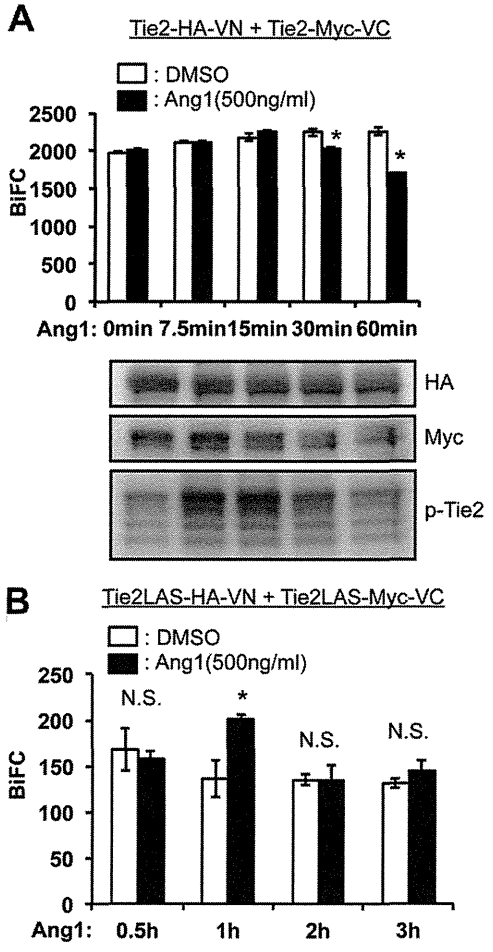

FIGURE 5. **BiFC analysis of ligand-dependent dimerization of Tie2.** *A*, dimerization of Tie2 was observed in Tie2-VN- and Tie2-VC-coexpressing NIH3T3 cells in the presence or absence of Angl stimulation. At each time point, cell lysates were analyzed for Tie2-HAVN and Tie2-MycVC as well as the degree of Tie2 phosphorylation (*lower panel*). Note that Angl stimulation did not enhance BiFC level but rather attenuated it 30 min after stimulation with Angl. *B*, time course of dimerization of Tie2YIA/LAS (Tie2LAS) was observed in Tie2 YIA/LAS-VN- and Tie2 YIA/LAS -VC-coexpressing HEK293T cells in the presence or absence of Angl stimulation (*, $p < 0.05$; $n = 3$). *DMSO*, dimethyl sulfoxide; *N.S.*, not significant.

DISCUSSION

In the present study, we visualized Tie2 dimerization by the BiFC method and sought ligand-independent dimerization domains of Tie2. A previous report showed that Tie2 clusters are expressed on the apical and basolateral plasma membranes (19). However, it was not clear whether Tie2 phosphorylation results in dimer formation. Here, we showed that kinase-inactive Tie2 mutants also form dimers in the absence of Angl. Thus, Tie2 can indeed form dimers without Angl. To analyze the role of ligand-independent dimerization of Tie2, a mutant that cannot form dimers in the absence of Angl is required. In the present study, we utilized a mutant with no evidence of Tie1-Tie1 dimerization even when overexpressed. Based on the amino acid sequence difference between Tie2 and Tie1, we found that YIA in the Tie2 cytoplasmic domain is important for ligand-independent Tie2 dimerization.

We show that the YIA domain required to form ligand-independent Tie2 dimers is situated between the catalytic and activation loops in the intracellular region of the molecule. Previ-

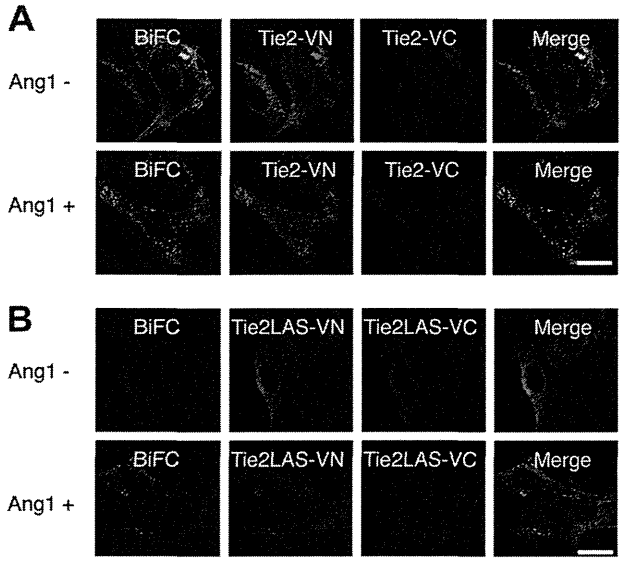

FIGURE 6. **Tie2YIA/LAS cannot form ligand-independent dimers but is dimerized and phosphorylated upon stimulation with Ang1.** *A*, dimerization and localization of Tie2 were observed in Tie2-VN- and Tie2-VC-coexpressing NIH3T3 cells in the presence or absence of Ang1. Wild-type Tie2 can form dimers irrespective of Ang1 stimulation, as confirmed by BiFC. However, this dimerized Tie2 forms cluster-like aggregations and is internalized upon stimulation with Ang1. *B*, similar to *A*, dimerization and localization of Tie2YIA/LAS (Tie2LAS) is observed in Tie2YIA/LAS-VN- and Tie2YIA/LAS-VC-coexpressing NIH3T3 cells. In the absence of Ang1, Tie2LAS did not dimerize but formed cluster-like aggregations upon stimulation with Ang1. *Bar* indicates 20 μm.

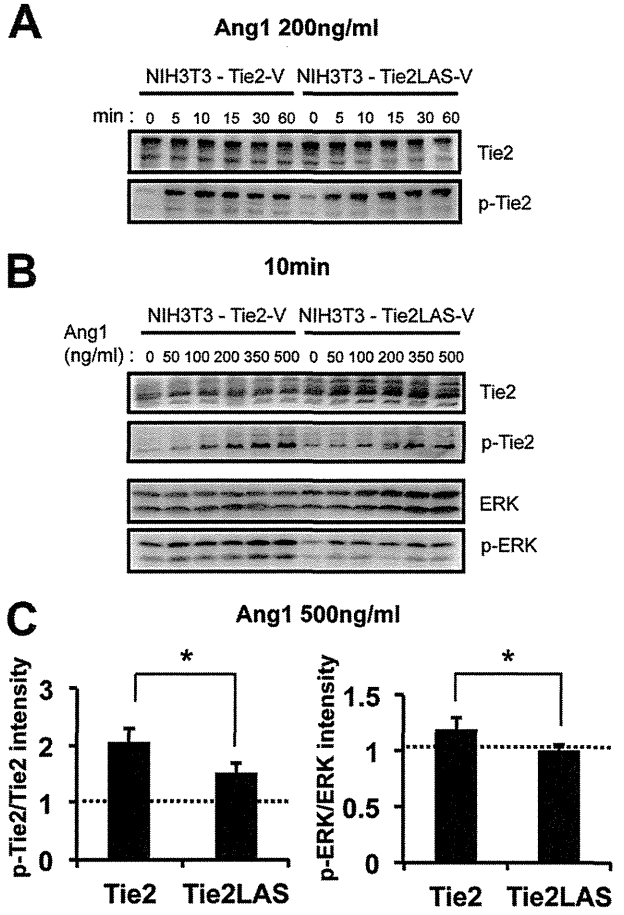

FIGURE 7. **Phosphorylation of Tie2 and Tie2 downstream molecule Erk.** *A*, Ang1 reactivity of Tie2 and Tie2YIA/LAS. After exposure to 200 ng/ml of Ang1, Tie2 and Tie2YIA/LAS phosphorylation was detected in a time-dependent fashion between 0 and 60 min. *B*, Ang1 reactivity of Tie2 and Tie2YIA/LAS. Ang1-mediated Tie2, Tie2YIA/LAS, and Erk phosphorylation was detected in a dose-dependent fashion between 0 and 500 ng/ml for 10 min. *C*, Tie2 and Erk phosphorylation on stimulation with 500 ng/ml Ang1 was quantified. The ratio of pTie2/Tie2 or pErk/Erk in cells on stimulation with Ang1 was compared with Ang1-untreated cells. (*, $p < 0.05$; $n = 3$).

ous reports show that the Tie2 C-terminal tail has a negative regulatory role in Tie2 signaling and function (31, 32). To activate Tie2, conformational changes in the intracellular loop structure and C-terminal tail are required for ATP and substrate binding. Therefore, it is possible that YIA domains control the movement of these loop and C-terminal tails. Further structural analysis of Tie2 will be necessary to assess how the YIA domain controls ligand-independent dimerization of Tie2 for folding and Tie2-Tie2 associations.

Unlike Tie2 homodimer formation, the BiFC method reveals that Tie2 and Tie1 scarcely interact. Recently, it has been reported that Tie2-Tie1 heterodimer formation is induced in the extracellular domain of Tie2 and Tie1, respectively, and that this occurs in the absence of angiopoietin ligation (33). Heterodimerization was observed using Tie receptors lacking intracellular domains. At present, it is difficult to explain this discrepancy, but it may simply be due to the absence of receptor cytoplasmic regions in the previous report. Indeed, when endogenous Tie2 and Tie1 localization in human umbilical vein endothelial cells was observed in the absence of Ang1, we found that Tie2 and Tie1 did not co-localize on the cell surface (supplemental Fig. S5). However, as previously reported, upon Ang1 stimulation, co-localization of these receptors does occur. In contrast, when NIH3T3 cells expressing Tie2-VN and Tie1*-VC were stimulated with Ang1, BiFC intensity was not enhanced (supplemental Fig. S6*A*). In addition, Ang1 activates both Tie2 and Tie1, but we did not observe a strong physical association between Tie2 and Tie1 in the immunoprecipitation analysis (supplemental Fig. S6, *B* and *C*). It has been reported that shedding of Tie1 extracellular domain itself induces Tie2 activation and that Ang2 acts as a Tie2 agonist upon Tie1 shedding (34–36). This suggests that Tie1 ectodomain shedding plays important roles in promoting Tie2 conformation changes and activation. Therefore, we cannot completely exclude the possibility that full-length Tie2 and Tie1 may heterodimerize under certain specific conditions in ECs.

It has been reported that Tie2 forms oligomers on the cell membrane (19); however, the function of such forms of Tie2 has not been elucidated. We found that a lack of ligand-independent dimerization of Tie2 led to attenuation of high dose Ang1-mediated activation of Tie2. This suggests that ligand-independent Tie2 dimerization plays a role in the rapid clustering of Tie2 upon activation with higher doses of Ang1 or in the preformation of Tie2 oligomers to respond to higher doses of Ang1. Further precise analysis of how ligand-independent dimerization of Tie2 relates to the extent of Tie2 phosphorylation at higher Ang1 doses is still required, including elucidation of the biological significance of Tie2 oligomers.

In humans, an amino acid substitution of tryptophan for arginine at residue (Tie2R849W) leads to ligand-independent constitutive activation; it is associated with familial venous malformations and causes thickness or lack of smooth muscle cells

in the veins systemically (14, 29, 37). In the present study, we showed that the intensity of BiFC signals from Tie2R848W-Tie2R848W was enhanced. Interestingly, Tie2R848W interactions with WT Tie2 were stronger than Tie2-Tie2 interactions. This suggests that Tie2R848W may heterodimerize with WT Tie2 and induce constitutive phosphorylation of WT Tie2. Therefore, analysis of regulatory mechanisms in ligand-independent dimerization domains may be useful for developing therapeutic strategies to inhibit Tie2 activation in patients suffering from venous malformation.

Acknowledgments—We thank T. Kamimoto, N. Fujimoto, and K. Fukuhara for technical assistance.

REFERENCES

1. Dejana, E., Tournier-Lasserve E., and Weinstein, B. M. (2009) The control of vascular integrity by endothelial cell junctions: molecular basis and pathological implications. *Dev. Cell* **16,** 209–221
2. Augustin, H. G., Koh, G. Y., Thurston, G., and Alitalo, K. (2009) Control of vascular morphogenesis and homeostasis through the angiopoietin-Tie system. *Nat. Rev. Mol. Cell Biol.* **10,** 165–177
3. Sato, T. N., Tozawa, Y., Deutsch, U., Wolburg-Buchholz, K., Fujiwara, Y., Gendron-Maguire, M., Gridley, T., Wolburg, H., Risau, W., and Qin, Y. (1995) Distinct roles of the receptor tyrosine kinases Tie-1 and Tie-2 in blood vessel formation. *Nature* **376,** 70–74
4. Davis, S., Aldrich, T. H., Jones, P. F., Acheson, A., Compton, D. L., Jain, V., Ryan, T. E., Bruno, J., Radziejewski, C., Maisonpierre, P. C., and Yancopoulos, G. D. (1996) Isolation of angiopoietin-1, a ligand for the TIE2 receptor, by secretion-trap expression cloning. *Cell* **87,** 1161–1169
5. Fukuhara, S., Sako, K., Minami, T., Noda, K., Kim, H. Z., Kodama, T., Shibuya, M., Takakura, N., Koh, G. Y., and Mochizuki, N. (2008) Differential function of Tie2 at cell-cell contacts and cell-substratum contacts regulated by angiopoietin-1. *Nat. Cell Biol.* **10,** 513–526
6. Saharinen, P., Eklund, L., Miettinen, J., Wirkkala, R., Anisimov, A., Winderlich, M., Nottebaum, A., Vestweber, D., Deutsch, U., Koh, G. Y., Olsen, B. R., and Alitalo, K. (2008) Angiopoietins assemble distinct Tie2 signalling complexes in endothelial cell-cell and cell-matrix contacts. *Nat. Cell Biol.* **10,** 527–537
7. Takakura, N., Watanabe, T., Suenobu, S., Yamada, Y., Noda, T., Ito, Y., Satake, M., and Suda, T. (2000) A role for hematopoietic stem cells in promoting angiogenesis. *Cell* **102,** 199–209
8. Dumont, D. J., Gradwohl, G., Fong, G. H., Puri, M. C., Gertsenstein, M., Auerbach, A., and Breitman, M. L. (1994) Dominant-negative and targeted null mutations in the endothelial receptor tyrosine kinase, tek, reveal a critical role in vasculogenesis of the embryo. *Genes Dev.* **8,** 1897–1909
9. Puri, M. C., Rossant, J., Alitalo, K., Bernstein, A., and Partanen, J. (1995) The receptor tyrosine kinase TIE is required for integrity and survival of vascular endothelial cells. *EMBO J.* **14,** 5884–5891
10. Puri, M. C., Partanen, J., Rossant, J., and Bernstein, A. (1999) Interaction of the TEK and TIE receptor tyrosine kinases during cardiovascular development. *Development* **126,** 4569–4580
11. Saharinen, P., Kerkelä, K., Ekman, N., Marron, M., Brindle, N., Lee, G. M., Augustin, H., Koh, G. Y., and Alitalo, K. (2005) Multiple angiopoietin recombinant proteins activate the Tie1 receptor tyrosine kinase and promote its interaction with Tie2. *J. Cell Biol.* **169,** 239–243
12. Yuan, H. T., Venkatesha, S., Chan, B., Deutsch, U., Mammoto, T., Sukhatme, V. P., Woolf, A. S., and Karumanchi, S. A. (2007) Activation of the orphan endothelial receptor Tie1 modifies Tie2-mediated intracellular signaling and cell survival. *FASEB J.* **21,** 3171–3183
13. Patan, S. (1998) TIE1 and TIE2 receptor tyrosine kinases inversely regulate embryonic angiogenesis by the mechanism of intussusceptive microvascular growth. *Microvasc. Res.* **56,** 1–21
14. Morris, P. N., Dunmore, B. J., Tadros, A., Marchuk, D. A., Darland, D. C., D'Amore, P. A., and Brindle, N. P. (2005) Functional analysis of a mutant form of the receptor tyrosine kinase Tie2 causing venous malformations. *J. Mol. Med.* **83,** 58–63
15. Maisonpierre, P. C., Suri, C., Jones, P. F., Bartunkova, S., Wiegand, S. J., Radziejewski, C., Compton, D., McClain, J., Aldrich, T. H., Papadopoulos, N., Daly, T. J., Davis, S., Sato, T. N., and Yancopoulos, G. D. (1997) Angiopoietin-2, a natural antagonist for Tie2 that disrupts *in vivo* angiogenesis. *Science* **277,** 55–60
16. Thomas, M., and Augustin, H. G. (2009) The role of the Angiopoietins in vascular morphogenesis. *Angiogenesis* **12,** 125–137
17. Eklund, L., and Olsen, B. R. (2006) Tie receptors and their angiopoietin ligands are context-dependent regulators of vascular remodeling. *Exp. Cell Res.* **312,** 630–641
18. Kim, I., Kim, J. H., Moon, S. O., Kwak, H. J., Kim, N. G., Koh, G. Y. (2000) Angiopoietin-2 at high concentration can enhance endothelial cell survival through the phosphatidylinositol 3'-kinase/Akt signal transduction pathway. *Oncogene* **19,** 4549–4552
19. Bogdanovic E., Coombs N., and Dumont D. J. (2009) Oligomerized Tie2 localizes to clathrin-coated pits in response to angiopoietin-1. *Histochem. Cell Biol.* **132,** 225–237
20. Jura, N., Endres, N. F., Engel, K., Deindl, S., Das, R., Lamers, M. H., Wemmer, D. E., Zhang, X., and Kuriyan, J. (2009) Mechanism for activation of the EGF receptor catalytic domain by the juxtamembrane segment. *Cell* **137,** 1293–1307
21. Red Brewer, M., Choi, S. H., Alvarado, D., Moravcevic, K., Pozzi, A., Lemmon, M. A., and Carpenter, G. (2009) The juxtamembrane region of the EGF receptor functions as an activation domain. *Mol. Cell* **34,** 641–651
22. Yu, X., Sharma, K. D., Takahashi, T., Iwamoto, R., and Mekada, E. (2002) Ligand-independent dimer formation of epidermal growth factor receptor (EGFR) is a step separable from ligand-induced EGFR signaling. *Mol. Biol. Cell* **13,** 2547–2557
23. Tao, R. H., and Maruyama, I. N. (2008) All EGF (ErbB) receptors have preformed homo- and heterodimeric structures in living cells. *J. Cell Sci.* **121,** 3207–3217
24. Livnah, O., Stura, E. A., Middleton, S. A., Johnson, D. L., Jolliffe, L. K., and Wilson, I. A. (1999) Crystallographic evidence for preformed dimers of erythropoietin receptor before ligand activation. *Science* **283,** 987–990
25. Chan, F. K., Chun, H. J., Zheng, L., Siegel, R. M., Bui, K. L., and Lenardo, M. J. (2000) A domain in TNF receptors that mediates ligand-independent receptor assembly and signaling. *Science* **288,** 2351–2354
26. Kerppola, T. K. (2006) Design and implementation of bimolecular fluorescence complementation (BiFC) assays for the visualization of protein interactions in living cells. *Nat. Protocols* **1,** 1278–1286
27. Morita, S., Kojima, T., and Kitamura, T. (2000) Plat-E: an efficient and stable system for transient packaging of retroviruses. *Gene Ther.* **7,** 1063–1066
28. Saitoh, T., Nakano, H., Yamamoto, N., and Yamaoka, S. (2002) Lymphotoxin-β receptor mediates NEMO-independent NF-κB activation. *FEBS Lett.* **532,** 45–51
29. Vikkula, M., Boon, L. M., Carraway, K. L., 3rd, Calvert, J. T., Diamonti, A. J., Goumnerov, B., Pasyk, K. A., Marchuk, D. A., Warman, M. L., Cantley, L. C., Mulliken, J. B., and Olsen, B. R. (1996) Vascular dysmorphogenesis caused by an activating mutation in the receptor tyrosine kinase TIE2. *Cell* **87,** 1181–1190
30. Bogdanovic, E., Nguyen, V. P., and Dumont, D. J. (2006) Activation of Tie2 by angiopoietin-1 and angiopoietin-2 results in their release and receptor internalization. *J. Cell Sci.* **119,** 3551–3560
31. Shewchuk, L. M., Hassell, A. M., Ellis, B., Holmes, W. D., Davis, R., Horne, E. L., Kadwell, S. H., McKee, D. D., and Moore, J. T. (2000) Structure of the Tie2 RTK domain: self-inhibition by the nucleotide binding loop, activation loop, and C-terminal tail. *Structure* **8,** 1105–1113
32. Niu, X. L., Peters, K. G., and Kontos, C. D. (2002) Deletion of the carboxyl terminus of Tie2 enhances kinase activity, signaling, and function. Evidence for an autoinhibitory mechanism. *J. Biol. Chem.* **277,** 31768–31773
33. Seegar, T. C., Eller, B., Tzvetkova-Robev, D., Kolev, M. V., Henderson, S. C., Nikolov, D. B., and Barton, W. A. (2010) Tie1-Tie2 interactions mediate functional differences between angiopoietin ligands. *Mol. Cell* **37,** 643–655
34. Yabkowitz, R., Meyer, S., Black, T., Elliott, G., Merewether, L. A., and Yamane, H. K. (1999) Inflammatory cytokines and vascular endothelial

growth factor stimulate the release of soluble tie receptor from human endothelial cells via metalloprotease activation. *Blood* **93,** 1969–1979

35. Marron, M. B., Singh, H., Tahir, T. A., Kavumkal, J., Kim, H. Z., Koh, G. Y., and Brindle, N. P. (2007) Regulated proteolytic processing of Tie1 modulates ligand responsiveness of the receptor-tyrosine kinase Tie2. *J. Biol. Chem.* **282,** 30509–30517
36. Singh, H., Milner, C. S., Aguilar Hernandez, M. M., Patel, N., and Brindle, N. P. (2009) Vascular endothelial growth factor activates the Tie family of receptor tyrosine kinases. *Cell Signal.* **21,** 1346–1350
37. Limaye, N., Wouters, V., Uebelhoer, M., Tuominen, M., Wirkkala, R., Mulliken, J. B., Eklund, L., Boon, L. M., and Vikkula, M. (2009) Somatic mutations in angiopoietin receptor gene TEK cause solitary and multiple sporadic venous malformations. *Nat. Genet.* **41,** 118–124

The American Journal of Pathology, Vol. 182, No. 5, May 2013

ELSEVIER

The American Journal of
PATHOLOGY

ajp.amjpathol.org

TUMORIGENESIS AND NEOPLASTIC PROGRESSION

Possible Role of Mural Cell–Covered Mature Blood Vessels in Inducing Drug Resistance in Cancer-Initiating Cells

Takahiro Matsui,*† Yumi Kinugasa,* Hidekazu Tahara,*‡ Yuzuru Kanakura,† and Nobuyuki Takakura*§

From the Department of Signal Transduction, Research Institute for Microbial Diseases, and the Department of Hematology and Oncology,† Osaka University Graduate School of Medicine, Osaka University, Osaka; the Department of Urology,‡ Kyoto Prefectural University of Medicine, Kyoto; and Japan Science and Technology Agency (JST),§ K's Gobancho, Tokyo, Japan*

Accepted for publication January 7, 2013.

Address correspondence to Nobuyuki Takakura, M.D., Ph.D., Department of Signal Transduction, Research Institute for Microbial Diseases, Osaka University, 3-1 Yamadaoka, Suita, Osaka 565-0871, Japan. E-mail: ntakaku@biken.osaka-u.ac.jp.

Cancer recurrence has been suggested to be induced by residual cancer-initiating cells (CICs) or cancer stem cells (CSCs) after chemotherapy. Moreover, it is possible that CICs/CSCs acquire more aggressive behavior after therapy as shown by invasion and metastasis. In the cancer microenvironment, CICs/CSCs may localize in a specific area, the so-called stem cell niche, and isolation of this niche is important to elucidate the molecular mechanism of how CICs/CSCs acquire malignancy. We analyzed whether CICs acquire drug resistance after cancer drug treatment in a tumor cell allograft model in which we could identify and isolate living CICs by detecting a higher level of transcriptional activity of the *PSF1* gene promoter. In our models using Lewis lung carcinoma (LLC) mouse lung cancer and colon26 mouse colon cancer cell lines, we found that CICs in both tumors acquired drug resistance after cancer drug treatment. Interestingly, response to the anticancer drug was quite different between LLC and colon26 original tumors (ie, the proportion of CICs in LLC tumors increased but in colon26 tumors the proportion decreased). We found that CICs frequently localized near mature blood vessels in which endothelial cells were covered with mural cells and that the incidence of mature blood vessels in LLC tumors was four times higher than in colon26 tumors. These results suggest a relationship between mature blood vessels and CIC drug resistance. *(Am J Pathol 2013, 182: 1790–1799; http://dx.doi.org/10.1016/j.ajpath.2013.01.019)*

A recent concept has suggested that the recurrence of cancer is induced by cancer-initiating cells (CICs)/cancer stem cells (CSCs) that are resistant to conventional chemoradiotherapy.[1,2] They are defined as malignant cancer cells. Moreover, cells in this population have a greater ability to spread to other organs to form metastatic lesions and to digest matrices for invasion even during chemotherapy. In addition, a poor prognosis in a diverse set of human and mouse malignancies was associated with the expression of an embryonic stem cell–like genetic program,[3–5] suggesting that CSCs express an embryonic stem cell–specific genetic code. There is no doubt that CSC death is crucial for a permanent cancer cure.

It is widely accepted that CSCs/CICs have multidrug resistance and radiotherapy resistance mediated by activation of DNA damage responses.[6] In addition, the association of CSCs/CICs with the expression of multidrug-resistant genes was reported.[7] For example, ABCB5 is well known to play a role in drug resistance, and is one of a number of molecules proposed as a marker of CSC melanoma.[7,8] In a human breast cancer cell line, ABCB1 is co-regulated with CD44 expression (one of the CSC markers).[9] Moreover, it was reported that CD133, which is used as a stem cell marker, promotes up-regulation of ABCB1 and higher ABC transporter activity in rat glioma cells.[10] Another possibility is that cancer stromal cells in the tumor microenvironment prevent CSC cell death by several cues through the interaction between CSCs and stromal cells. In organs and tissues, the stem cell population localizes in a specific area, the so-called niche, and the interaction between stem cells and cells composing the niche is important to maintain the stemness of stem cells, such as self-renewal, immature status, and dormancy in such a niche.[11]

In the field of hematopoiesis, the niche has been analyzed extensively. The vascular niche was suggested to be important

Supported by a Grant-in-Aid for Scientific Research from the Ministry of Education, Culture, Sports, Science and Technology and the Japan Society for the Promotion of Science of Japan.

http://dx.doi.org/10.1016/j.ajpath.2013.01.019

for self-renewal of hematopoietic stem cells (HSCs) because proliferation of HSCs was observed in vascular areas in embryos and in adult bone marrow.[12,13] On the other hand, HSC quiescence is induced in the osteoblastic niche where osteoblasts adhere to endosteum in the bone marrow.[14] Several tumor models have proposed that CSCs also may localize in vascular areas.[15,16] In a skin cancer model, vascular endothelial growth factor derived from CSCs expanded the vascular area, including the number of blood vessels, and resulted in the proliferation of CSCs.[17] On the other hand, although not connected with the localization of CSCs, it has been suggested that hepatocyte growth factor derived from myofibroblasts maintains the stemness of CSCs in colon cancer indirectly via the frizzled/Wnt pathway and that myofibroblast-secreted factors play pivotal roles in the induction of cancer cells into malignant CSCs.[18] Myofibroblasts are α-smooth muscle actin (α-SMA)–positive cells that usually localize near blood vessels and may work as a mural cell population. Therefore, based on previous reports, the vascular niche in which endothelial cells are covered with α-SMA–positive cells may maintain the stemness of CSCs; however, this has not been verified yet. Therefore, it is important to evaluate whether mural cell–covered blood vessels work as a niche for CSC/CICs.

For the evaluation of drug resistance, CSCs or CICs should be isolated as living cells from the tumor that has remained after therapy and it should be observed whether those cell types indeed do form secondary tumors. Several methods have been suggested for the detection of CSCs/CICs (ie, surface expression of CD133, surface-high expression of CD44 and negative-low expression of CD24, and high aldehyde dehydrogenase activity). However, data obtained by these methods have not always resulted in the same conclusion in mice. Therefore, we have generated a new technique to identify CICs by using promoter activity of the partner of sld five 1 (*Psf1*) gene (PSF1-promoter), a member of the GINS complex (from the Japanese go-ichi-ni-san meaning 5-1-2-3, derived from four related subunits of the complex Sld5, Psf1, Psf2 and Psf3), which is required for DNA replication by associating with CDC45 in yeast.[19] PSF1 protein is composed of coiled-coil, arginine-rich, and PEST-like domains from the N to the C terminus, and the C-terminal domain of PSF1 is crucial for chromatin binding and replication activity.[20] PSF1 expression was observed abundantly in bone marrow, thymus, and testis in mice.[21] Immature cell populations and stem cell populations express PSF1 [ie, epiblasts during embryogenesis, bone marrow hematopoietic stem cell populations, sperm stem cells (spermatogonia), and others] in mice.[21–23] Based on the phenotypes of mutant mice, PSF1 expression was required for acute proliferation of immature cell types such as epiblasts in embryos[21] and HSCs after bone marrow ablation.[23] The PSF1 in mice comprises the GINS complex, as observed in yeast. Therefore, it is possible that PSF1 is involved in the formation of DNA replication in mammals; however, the function of PSF1 has not been clarified in mice yet.

We found that promoter activity of the *Psf1* gene correlated with cancer cell malignancy.[16] When cells containing high or low levels of PSF1-promoter activity were compared, PSF1-promoter^{high} cancer cells had high proliferative activity, serial transplantation potential, and metastatic ability. Moreover, PSF1-promoter^{high} cancer cells displayed embryonic stem cell–like gene expression signatures. These results suggest that PSF1-promoter^{high} cancer cells are CICs. In the present work, we analyzed the *in vitro* and *in vivo* drug resistance of PSF1-promoter^{high} cancer cells and analyzed the microenvironment that supports the drug resistance of PSF1-promoter^{high} cancer cells.

Materials and Methods

Cell Culture

Lewis lung carcinoma (LLC) cells or colon26 (mouse colon cancer) cells were maintained in Dulbecco's modified Eagle's medium (Sigma-Aldrich, St. Louis, MO) or RPMI 1640 (Sigma-Aldrich), respectively, with 10% fetal bovine serum (Equitech-Bio, Kerville, TX) and penicillin/streptomycin. Colon26 cells or LLC cells expressing enhanced green fluorescent protein (EGFP) under the transcriptional control of the PSF1-promoter (colon26-*PSF1p-EGFP* or LLC-*PSF1p-EGFP*) were generated as previously reported.[16]

Mice

Seven- to 8-week-old C57BL/6 female mice (for LLC experiments), BALB/c female mice of the same age (for colon26 experiments), and 6- to 7-week-old KSN female nude mice were purchased from Japan SLC (Shizuoka, Japan). All animal studies were approved by the Osaka University Animal Care and Use Committee. Subcutaneous allografts were established by injecting 10^6 cells into the backs of mice. Tumor volume was measured with a caliper and calculated according to the following formula: V = width × width × length × 0.5.

Anticancer Agent Administration

On day 7 after subcutaneous inoculation of cancer cells as described earlier, mice were treated with intraperitoneal injections of saline, 60 mg/kg body weight 5-fluorouracil (5-FU; Kyowa Hakko Kirin, Tokyo, Japan), or 5 mg/kg body weight cisplatin (Bristol-Myers, Tokyo, Japan) every other day. LLC-*PSF1p-EGFP*–bearing mice were administered five treatments with 5-FU and the other mice received four treatments with either saline or cisplatin. Flow cytometric analysis or fluorescence-activated cell sorting was performed 3 days after the last administration of an anticancer agent.

Flow Cytometric Analysis and Cell Sorting

Mice were euthanized and tumor tissues were excised, minced, and digested with Dispase II (Godo Shusei, Corp., Chiba, Japan) and collagenase (Wako, Osaka, Japan) with continuous shaking at 37°C. Single-cell suspensions of

tumor cells were prepared using a standard protocol.[16] Flow cytometric analysis was performed using a FACSCalibur (Becton Dickinson, Franklin Lakes, NJ), and cell sorting was performed using a FACSAria (Becton Dickinson). For the EGFP-high cell population, 5% of the most brightly fluorescing cells were sorted, and for the EGFP-low cell population, 5% of the least fluorescent cells were sorted. We used parental LLC or colon26 as negative controls.

In Vitro Colony Formation Analysis and *in Vivo* Tumor Initiation Analysis

Isolated cells were plated at a concentration of 500 cells per dish on 10-cm culture dishes and cultured in culture media with or without various doses of anticancer agents. For *in vivo* experiments, sorted cells were suspended in 100 μL of PBS with growth factor–reduced Matrigel (BD Biosciences, San Jose, CA) and injected subcutaneously into the mice. Tumorigenic ability was judged for 8 weeks after inoculation of tumor cells.

Immunohistochemistry

Dissected tissues were fixed in 4% paraformaldehyde and dehydrated in methanol. Fixed specimens were embedded in polyester wax (VWR International, Ltd., Lutterworth, UK) and cut into 7-μm sections as described.[24] The staining procedure of tissue sections was almost the same as previously reported.[25] Rabbit anti-GFP antibody (Invitrogen, Eugene, OR), rat anti-CD31 antibody (BD Biosciences), and mouse anti–α-SMA antibody (Sigma-Aldrich) were used for primary antibodies.

For the immunohistochemical analyses, biotin-conjugated goat anti-rabbit Ig (Dako, Carpinteria, CA) or biotin-conjugated goat anti-rat Ig (Invitrogen) was used as a secondary antibody. The Vectastain ABC Kit (Vector Laboratories, Burlingame, CA) was used to amplify the target antigen signal before the visualization of horseradish peroxidase by diaminobenzidine (Dojindo, Kumamoto, Japan). The 5-bromo-4-chloro-3-indoxyl phosphate and nitro blue tetrazolium chloride substrate system (Dako) was used for the visualization of alkaline phosphatase.

For the immunofluorescence analyses, Alexa Fluor 488–conjugated IgGs (Invitrogen) or streptavidin-allophycocyanin (APC) conjugate (BD Pharmingen, Franklin Lakes, NJ) was used as a second-step reagent. Images were acquired using a DFC 500 digital camera (Leica Microsystems, Nussloch, Germany) and processed with the Leica application suite and Adobe Photoshop CS2 software (Tokyo, Japan). All images shown are representative of three to six independent experiments.

Statistical Analysis

Results are expressed as the means ± SEM. The Student's *t*-test was used for statistical analysis except for the cumulative survival rate data, for which the log-rank test was used. Differences were considered statistically significant when the P value was less than 0.05.

Results

PSF1 Promoter Activity Does Not Affect Drug Sensitivity Directly in Colon26 and LLC Cells

We previously designated *PSF1*-promoter^{high} cancer cells as a population of CICs/CSCs in a mouse tumor cell allograft model because they had higher tumorigenic, invasive, and metastatic abilities compared with *PSF1*-promoter^{low} cancer cells and had an embryonic stem cell–specific immature gene signature.[16] First, we observed whether *PSF1*-promoter^{high} cancer cells showed drug resistance. We used colon cancer (colon26) cell lines and lung cancer (LLC) cell lines that stably expressed EGFP under the transcriptional control of the *PSF1*-promoter (colon26- and LLC-*PSF1p-EGFP*, respectively). In these cells, the intensity of EGFP is correlated with endogenous *PSF1* mRNA expression.[16] After inoculation of colon26- or LLC-*PSF1p-EGFP*, tumors were dissected and EGFP-high (5% most bright) or EGFP-low (5% least bright) cancer cells were sorted by a fluorescence-activated cell sorter (Figure 1, A and B). Sorted cells were cultured for 10 days in culture media containing various doses of 5-FU. As previously reported, EGFP-high cells formed significantly larger colonies, as well as a higher number of colonies, compared with EGFP-low cells for both colon26 and LLC cells (Figure 1, C and D). The number of colonies formed by both EGFP-high and EGFP-low cells decreased in a dose-dependent manner in the presence of 5-FU. At a glance, EGFP-low cells seemed to be more sensitive to 5-FU because colonies were not formed at higher doses of 5-FU. However, when the sensitivity to 5-FU was evaluated by the relative ratio of the number of colonies in the presence of 5-FU to that in the absence of 5-FU, no significant differences in sensitivity to 5-FU were observed between EGFP-high and EGFP-low cells (Figure 1, E and F). Therefore, we concluded that *PSF1*-promoter activity does not alter the drug sensitivity of the original cancers before 5-FU treatment, at least in colon26 and LLC cancer cells.

Expression Pattern of *PSF1* Promoter Activity in Remaining Cancer Cells after Treatment with Cancer Drug Is Different Depending on Cancer Cell Type

We next observed the level of *PSF1*-promoter activity in cancer cells after administration of a cancer drug in an allograft model using colon26- and LLC-*PSF1p-EGFP* cells. The administration of 5-FU *in vivo* had a marked cytoreductive effect in both tumors (Figure 2, A and B). However, there were obvious differences in EGFP fluorescence intensity of the residual cancer cells between colon26- and LLC-*PSF1p-EGFP* cells. In the case of colon26-*PSF1p-EGFP* cells, with 5-FU administration *in vivo* there was a marked

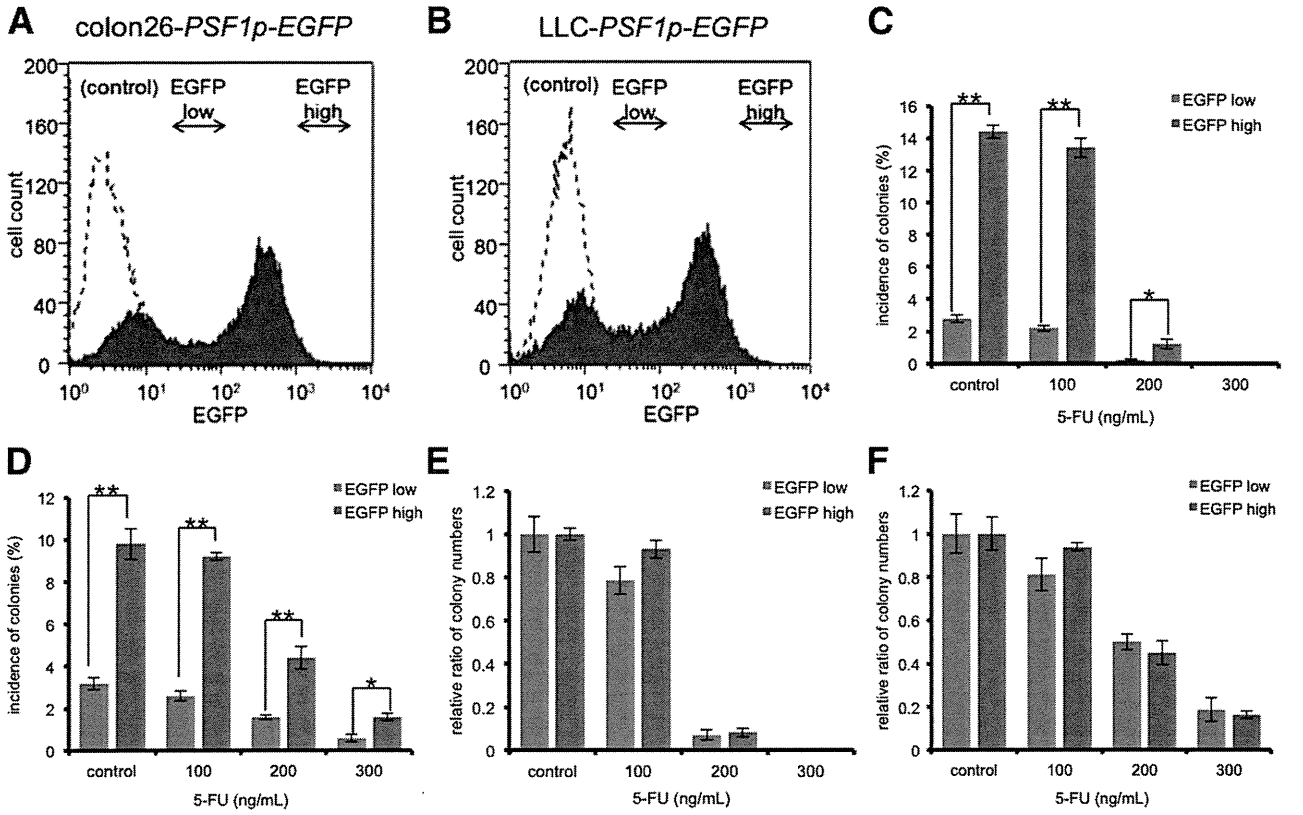

Figure 1 *PSF1*-promoter activity does not affect drug sensitivity directly in colon26 and LLC cells. **A**: Flow cytometric analysis of cells from tumor tissues. Tumors were derived from mice injected with colon26 (control: **dashed line**) or colon26-*PSF1p-EGFP* (**purple area**) cells (10^6 cells). **B**: Same experiment as described in **A** using LLC (control: **dashed line**) or LLC-*PSF1p-EGFP* (**purple area**) cells. **C** and **D**: Drug resistance analysis of sorted cells. Five hundred sorted cells as in **A** and **B**, respectively, were seeded onto 10-cm culture dishes and cultured in various dosages of 5-FU for 10 days. Colonies generated from different fractions were stained with Giemsa solution and assessed quantitatively. Data show the means ± SEM. $^*P < 0.05$, $^{**}P < 0.01$ ($n = 3$). **E** and **F**: Sensitivity to 5-FU. The relative ratio of the number of colonies in the presence of 5-FU to those in the absence of 5-FU obtained in experiments shown in **C** and **D**, respectively, was evaluated quantitatively. Data show the means ± SEM ($n = 3$).

reduction in the proportion of EGFP-high cells compared with the control group (Figure 2C). On the other hand, with LLC-*PSF1p-EGFP* cells, the proportion of EGFP-high cells increased after 5-FU administration in comparison with the control group (Figure 2D). Similar results were obtained with the administration of cisplatin (Supplemental Figure S1, A and B). These results showed a difference in the expression pattern of *PSF1*-promoter activity in residual cancer cells after cancer drug administration, depending on the cancer cell type.

PSF1-Promoter^{high} Cancer Cells Acquire Drug Resistance after Cancer Drug Administration

We previously reported that *PSF1*-promoter^{high} cancer cells had significantly higher tumorigenic activity than *PSF1*-promoter^{low} cancer cells.[16] We next assessed whether residual EGFP-high cancer cells after treatment with an anticancer drug (5-FU) in a tumor allograft model also would show tumor initiation activity and drug resistance in a second *in vitro* treatment with an anticancer drug. As shown in Figure 3A, LLC-*PSF1p-EGFP* cells were inoculated into mice and tumor-bearing mice were treated with 5-FU using the same schedule as described in Figure 2C. On day 18, tumors were dissected and two fractions of cancer cells (EGFP-low and EGFP-high cells) were sorted by a fluorescence-activated cell sorter as indicated (Figure 3A). Cancer cells (50, 100, or 1000) secondarily were inoculated into mice for observation of tumor initiation capacity. Moreover, cells were cultured in the presence or absence of 5-FU for 14 days and drug resistance was evaluated by calculating the number of colonies.

A smaller number of EGFP-high cells generated a secondary tumor more effectively than similar numbers of EGFP-low cells (Table 1). The difference in tumor initiation capacity between EGFP-low cells and EGFP-high cells was significant. When cultured in the presence or absence of 5-FU, EGFP-high cells formed significantly larger as well as a higher number of colonies than EGFP-low cells under all conditions (Figure 3B). In an evaluation of the sensitivity to 5-FU by the relative ratio of the number of colonies in the presence of 5-FU to those in the absence of 5-FU, EGFP-high cells showed significant resistance to 5-FU compared with EGFP-low cells (Figure 3C).

When EGFP-high or -low cells from tumors generated by colon26-*PSF1p-EGFP* cells were sorted on day 16 after

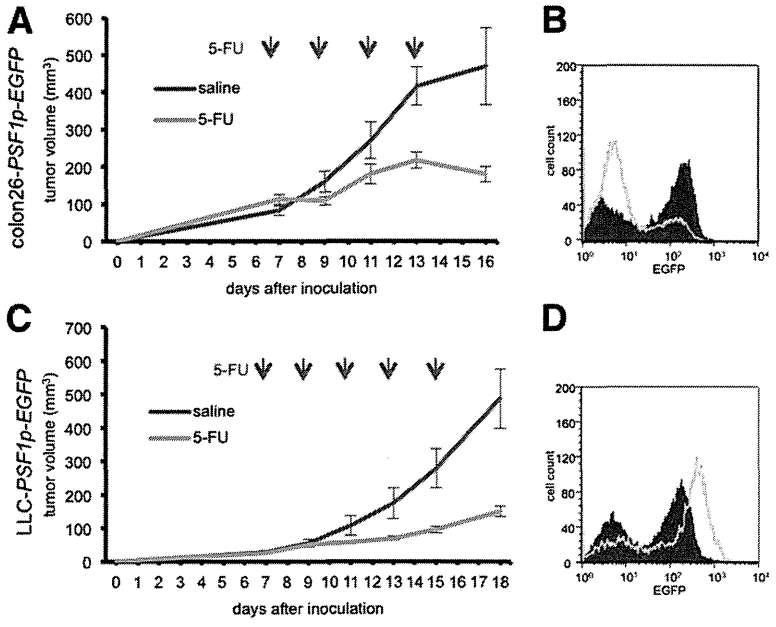

Figure 2 Expression pattern of *PSF1*-promoter activity in cancer cells that remain after treatment with cancer drug. **A:** Time course of tumor volume after 5-FU administration *in vivo*. 5-FU was administered to tumor-bearing mice inoculated by colon26-*PSF1p-EGFP* cells on days 7, 9, 11, and 13 as indicated by **red arrows**. Data show the means ± SEM ($n = 6$). **B:** Flow cytometric analysis of cells from tumor tissues on day 16 (as in **A**). Data obtained by flow cytometry in the saline (control) group (**purple area**) and the 5-FU–injected group (**green line**) represent the results of multiple experiments. **C:** Time course of tumor volume after 5-FU administration *in vivo*. 5-FU was administered to tumor-bearing mice inoculated by LLC-*PSF1p-EGFP* cells on days 7, 9, 11, 13, and 15 as indicated by **red arrows**. Data show the means ± SEM ($n = 7$). **D:** Flow cytometric analysis of cells from tumor tissues on day 18 (as in **C**). Data obtained by flow cytometry in the saline (control) group (**purple area**) and the 5-FU–injected group (**green line**) represent the results of multiple experiments.

administration of 5-FU using the same schedule as described in Figure 2 and cultured in the presence or absence of 5-FU, EGFP-high cells showed significant resistance to 5-FU compared with EGFP-low cells (Supplemental Figure S2, A–C) as observed in LLC tumors. EGFP-high cells and EGFP-low cells from non–5-FU–treated tumors did not show any differences in terms of drug resistance (Figure 1, E and F). This suggests that EGFP-high cells acquired drug resistance by the *in vivo* treatment with the cancer drug and became more malignant cancer cells, although their behavior was originally that of CICs/CSCs.

LLC Tumors, But Not Colon26 Tumors, Contain Abundant Mural Cell–Covered Mature Blood Vessels

In the case of an allograft model using colon26-*PSF1p-EGFP* cells, the proportion of EGFP-high cells decreased after 5-FU treatment as described earlier (Figure 2C), which was completely opposite of the result using LLC-*PSF1p-EGFP* cells (Figure 2D). These results suggest that the microenvironment in LLC tumors more effectively induced cancer cells to become drug resistant. Therefore, we next analyzed the characteristics of the tumor microenvironment, focusing especially on tumor vessels, because the vascular niche may be a key to the regulation of stemness of CSCs.[15,26]

In colon26 tumors the vascular density was high (Figure 4, A and C). However, most of the blood vessels were composed of endothelial cells alone and α-SMA–positive mural cell coverage of endothelial cells barely was observed. On the other hand, in case of LLC tumors, vascular density was not largely different from that in colon26 tumors, however, most of the blood vessels were covered with α-SMA–positive mural cells (Figure 4, B and D, and Supplemental Figure S3, A and B). The number of mural cells that covered blood vessels was four times higher in LLC tumors compared with colon26 tumors (Figure 4E). To investigate whether the distribution of mural cell–covered blood vessels was affected by 5-FU treatment, we observed blood vessel formation in colon26 tumors and LLC tumors on days 16 and 18, respectively, under the same schedule as described in Figure 2. The results suggested no remarkable differences in tumor blood vessels before and after 5-FU treatment (Supplemental Figure S3, C and D).

LLC-PSF1p-EGFP-High Cells Localize in the Mural Cell–Covered Blood Vessel Area

In the case of an allograft model using LLC-*PSF1p-EGFP* cells, the proportion of EGFP-high cells increased after 5-FU treatment as described earlier (Figure 2D). The high frequency of mural cell–covered blood vessels in LLC tumors was significantly different compared with that in colon26 tumors. It is possible that mural cell–covered blood vessels play a role in the induction of drug resistance in *PSF1p*-EGFP-high CICs/CSCs. If so, EGFP-high cells may localize near mural cell–covered blood vessels. To assess this, the tissue distribution of EGFP-high cells in tumors with or without 5-FU treatment was examined. With lower magnification, a dark brownish area where EGFP-high cells exist with high density was located in the marginal zone of the tumor mass regardless of 5-FU treatment (Figure 5, A and B). In this area, dark blue mural cell–covered blood vessels were observed frequently. By using higher magnification, it was apparent that EGFP-high cells were located near blood vessels in which endothelial cells were fully covered with α-SMA–positive mural cells (Figure 5, C and D). These results indicate that cancer cells expressing high levels of PSF1 are localized mainly near mature tumor

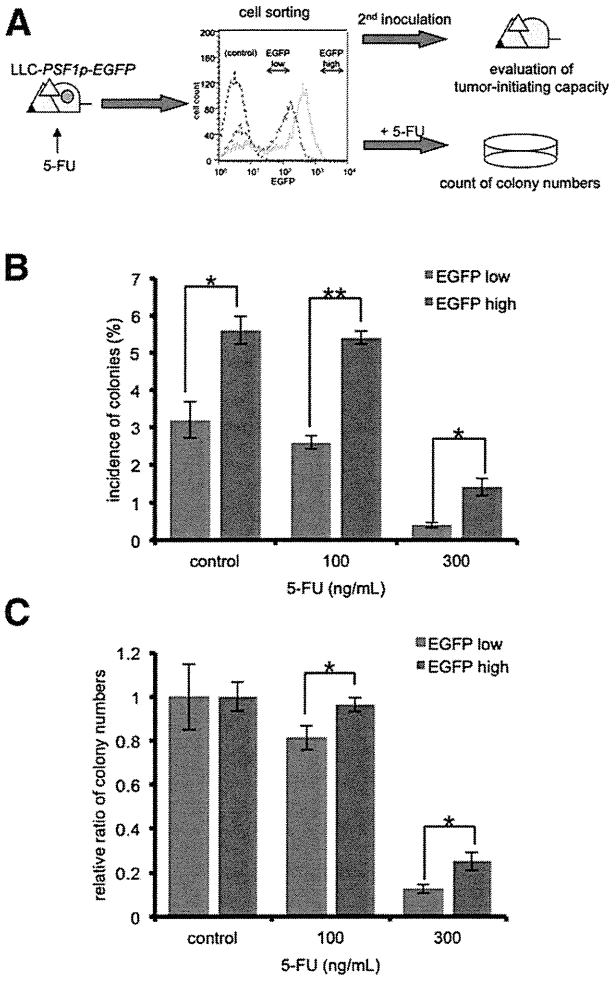

Figure 3 Acquisition of drug resistance after cancer drug administration. **A**: Analysis of the drug resistance capacity and tumor initiation capacity. Tumor-bearing mice by inoculation with LLC-*PSF1p-EGFP* cells were administered 5-FU as in Figure 2C. Tumor cells from the remaining tumor tissue were analyzed by flow cytometry and EGFP-high or EGFP-low cells were obtained. The **black line** shows LLC cells (no EGFP expression), the **red line** shows LLC-*PSF1p-EGFP* cells without 5-FU treatment, and the **green line** indicates LLC-*PSF1p-EGFP* cells treated with 5-FU *in vivo*. Cells from these two fractions were analyzed for *in vivo* tumorigenic activity and *in vitro* colony formation. **B**: Drug resistance analysis of residual cancer cells after 5-FU administration *in vivo*. Five hundred sorted cells as in **A** were seeded onto 10-cm culture dishes and cultured in various doses of 5-FU for 14 days. Colonies generated from different fractions were stained with Giemsa solution and assessed quantitatively. Data show the means ± SEM. $^*P < 0.05$, $^{**}P < 0.01$ ($n = 3$). **C**: Sensitivity to 5-FU. Relative ratio of the number of colonies in the presence of 5-FU to those in the absence of 5-FU obtained in experiment **B** was evaluated quantitatively. Data show the means ± SEM. $^*P < 0.05$ ($n = 3$).

blood vessels and that this microenvironment may contribute to cell survival and acquisition of drug resistance when tumors are exposed to anticancer agents.

Mature Blood Vessel Formation in Tumors Is Induced by Cancer Cells

Immunohistochemical analysis suggests that LLC cells induce mature blood vessel formation during tumorigenesis and that colon26 cancer cells cannot induce mature blood vessel formation abundantly. In summary, maturation of blood vessels appears to be induced depending on molecular cues from cancer cells, but not host cells. However, one of the most important concerns regarding our experimental systems is that the original hosts of the cancer cell lines used were different (ie, BALB/c mice for colon26 cells and C57BL/6 mice for LLC cells). Therefore, it is possible that the maturation of tumor blood vessels is affected by the strain of mouse. To test this possibility, a tumor transplantation model using nude mice for both colon26 and LLC cells was utilized.

As shown in Figure 6, α-SMA–positive mural cell–covered blood vessels barely were observed in colon26 tumors but were observed abundantly in LLC tumors (Figure 6, A and B). Similar to the original hosts, the number of blood vessels covered with mural cells was four times higher in LLC tumors compared with colon26 tumors (Supplemental Figure S4). This suggests that the maturation of blood vessels in tumors is induced depending on the tumor cells themselves. Moreover, when 5-FU was administered in this model using the same schedule as described in Figure 2, tumor growth effectively was inhibited in both tumors (Figure 6, C and D). In addition, as observed in the response of the original host allograft model, we confirmed that the proportion of EGFP-high cells decreased in colon26 tumors but increased in LLC tumors (Figure 6, E and F).

Finally, we analyzed whether the difference in the proportion of residual cancer cells expressing high levels of PSF1 (EGFP-high cells) would affect therapeutic performance such as prolonged survival. Survival periods of nude mice bearing colon26- or LLC-*PSF1p-EGFP* cells were observed after 5-FU administration. Survival of mice bearing colon26 tumors, in which the EGFP-high cell population was reduced dramatically by 5-FU treatment, was prolonged significantly compared with mice that received no medication (Figure 6G). On the other hand, the mice bearing an LLC tumor, in which EGFP-high cells resided after treatment with 5-FU, did not survive longer than mice that received no medication (Figure 6H). These results indicate that the existence of residual cancer cells

Table 1 Tumor Initiation Rate in Serial Transplantation

LLC-*PSF1p-EGFP* cells	EGFP low	EGFP high
1000 cells	100% ($n = 5$)	100% ($n = 5$)
100 cells	70% ($n = 10$)	100% ($n = 10$)
50 cells	80% ± 6.7%* ($n = 10 \times 3$)	100% ± 0% ($n = 10 \times 3$)

A small number of sorted cells as indicated were inoculated subcutaneously into mice and tumor formation was observed until 8 weeks after tumor cell inoculation. Quantitative evaluation was conducted using 50 sorted cells. Experiments were performed three times with similar results. Data show the means ± SEM. Statistic evaluation was performed between data of 50 cells.
$^*P < 0.05$ ($n = 10$).

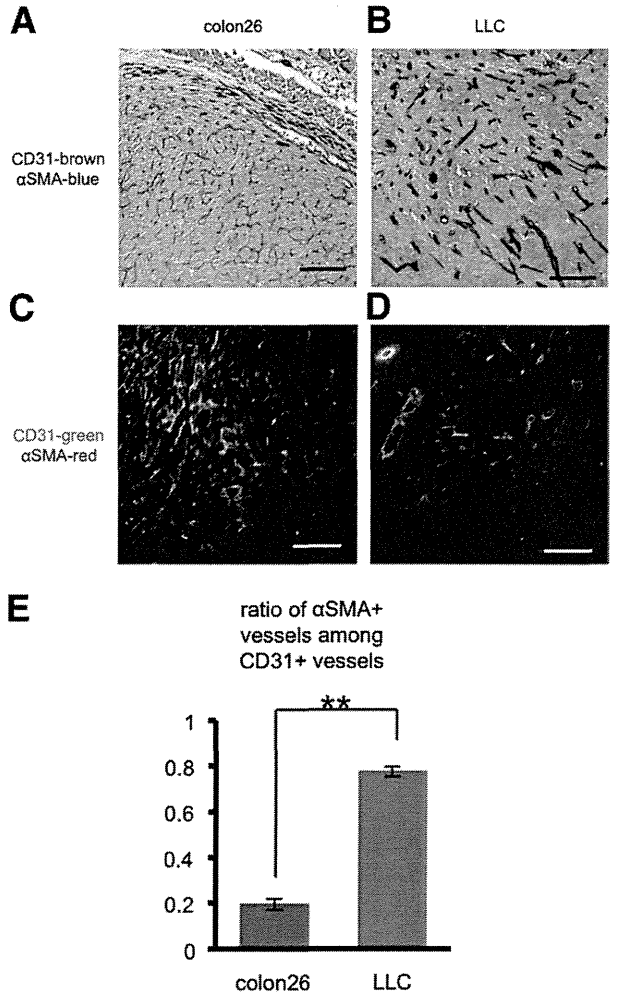

Figure 4 Immunohistochemical and immunofluorescence analyses of tumor vessels. **A** and **B**: Sections from colon26 (**A**) and LLC (**B**) tumors were double-stained with anti-CD31 antibody (brown) and anti–α-SMA antibody (blue). Scale bars: 200 μm. **C** and **D**: Sections from colon26 (**C**) and LLC (**D**) tumors were double-stained with anti-CD31 antibody (green) and anti–α-SMA antibody (red). Scale bars: 200 μm. **E**: The ratio of α-SMA–positive mural cell–covered blood vessels to all CD31-positive tumor vessels. Data are means ± SEM from five random fields. $^{**}P < 0.01$.

expressing high levels of PSF1 might be an important factor affecting prolonged survival.

Discussion

In this study, we analyzed the relationship between the tumor microenvironment and cancer cell malignancy using two different tumor cell types. The colon26 tumors produced abundant blood vessels; however, there were few mural cell–covered mature blood vessels. On the other hand, LLC tumors contained α-SMA–positive mural cell–covered mature blood vessels with high frequency. In normal organs, it was reported that the stem cell population self-renews in vascular areas.[27,28] It is possible that CICs/CSCs also localize in perivascular areas for self-renewal. Usually, blood vessels in normal organs are mural cell–covered mature blood vessels. Therefore, it is reasonable that mature blood vessels function as the vascular niche for stem cells. This suggests that a cancer microenvironment composed of abundant mature blood vessels, as in LLC tumors, may support the stemness of CSCs.

By using methods to identify malignant CICs by means of higher transcriptional activity of the *Psf1* gene, we found that drug resistance of CICs in original LLC or colon26 tumors was not largely different compared with *PSF1*-promoter^{low} cancer cells. However, after administration of an anticancer drug, residual *PSF1*-promoter^{high} CICs acquired drug resistance. In particular, the proportion of *PSF1*-promoter^{high} CICs increased in LLC tumors in which mature blood vessels were highly observed. Therefore, these results suggest that the microenvironment supports acquisition of drug resistance in cancer cells after anticancer drug administration and that mature blood vessels may be involved in this event.

The number of colonies derived from EGFP-high cells sorted from tumors decreased after *in vivo* 5-FU treatment (Figure 3B) compared with the number of colonies generated by cells of nontreated tumors (Figure 1D). Cells used in the experiment shown in Figure 3B already were exposed to 5-FU *in vivo*; thus, the condition of cells in Figure 1D is different from that of cells in Figure 3B. *PSF1*-promoter activity also may correlate with the cell cycle, and cycling cells are more affected by 5-FU *in vivo*. Here, it is emphasized that drug resistance by EGFP-high cells is induced after *in vivo* anticancer drug treatment.

Preliminary results suggest that among 5-FU–resistant genes, thymidylate synthase was up-regulated slightly in EGFP-high LLC cells after *in vivo* treatment with 5-FU compared with EGFP-low cells. Moreover, ABCB1 (MDR1) expression was up-regulated slightly without statistical significance. In terms of drug resistance, further precise analysis is required.

Recently, one report suggested that the population of CSCs in a tumor increased after treatment with an angiogenesis inhibitor.[29] The report suggested that hypoxia induced by the regression of blood vessels by an angiogenesis inhibitor activated the AKT signaling pathway in CSCs, resulting in the proliferation of CSCs. It is widely accepted that angiogenesis inhibitors normalize tumor blood vessels, resulting in effective induction of drug delivery into the parenchyma of a malignant tumor.[30] We previously showed that mural cell coverage of endothelial cells in tumors is induced by treatment with angiogenesis inhibitors.[31] In our present work, drug resistance of CICs was promoted effectively in tumors in which mature blood vessels abundantly were observed. Taken together, this suggests that expansion of CSCs after angiogenesis inhibitor treatment is associated with maturation of tumor blood vessels. In addition, it previously was reported that invasion of cancer cells was enhanced after angiogenesis inhibitor treatment in tumors.[32,33] To prevent normal blood vessels from damage, excessive amounts of angiogenesis inhibitor cannot be used. Because of this situation, mature blood vessels in tumors can survive. Considering that mature blood vessels may educate

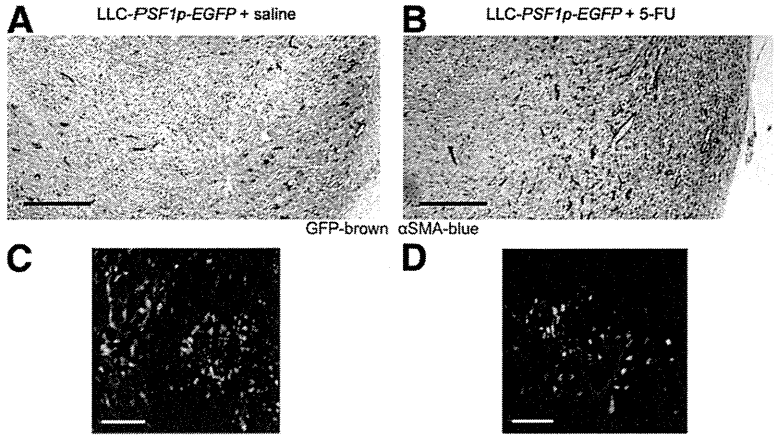

Figure 5 Localization of cancer cells with higher *PSF1*-promoter activity before and after 5-FU administration. **A** and **B**: LLC-*PSF1p-EGFP* cells subcutaneously inoculated into mice. Sections from tumor on day 18 as in Figure 2C with (**B**) or without (**A**) administration of 5-FU were double-stained with anti-GFP antibody (brown) and anti—α-SMA antibody (blue). Scale bar = 500 μm. **C** and **D**: Sections of tumor as in **A** or **B**, respectively, were stained with anti-GFP antibody (green), anti—α-SMA antibody (red), and anti-CD31 antibody (blue). Scale bars: 100 μm.

cancer cells to become aggressive cancer cells, the molecular mechanism of how blood vessels in tumors become mature should be elucidated.

In our present work, to clarify the involvement of mature blood vessels in the acquisition of malignant features by cancer cells, such as drug resistance, we tried to inhibit the transforming growth factor-β pathway. Because it has been reported that inhibition of the transforming growth factor-β signal suppressed mural cell—endothelial cell attachment,[34] we pursued this line of work to suppress mural cell coverage on endothelial cells in LLC tumors and analyzed whether the proportion of *PSF1p-EGFP*—high CICs decreased with 5-FU treatment. However, inhibition of the transforming growth factor-β signal suppressed angiogenesis itself and

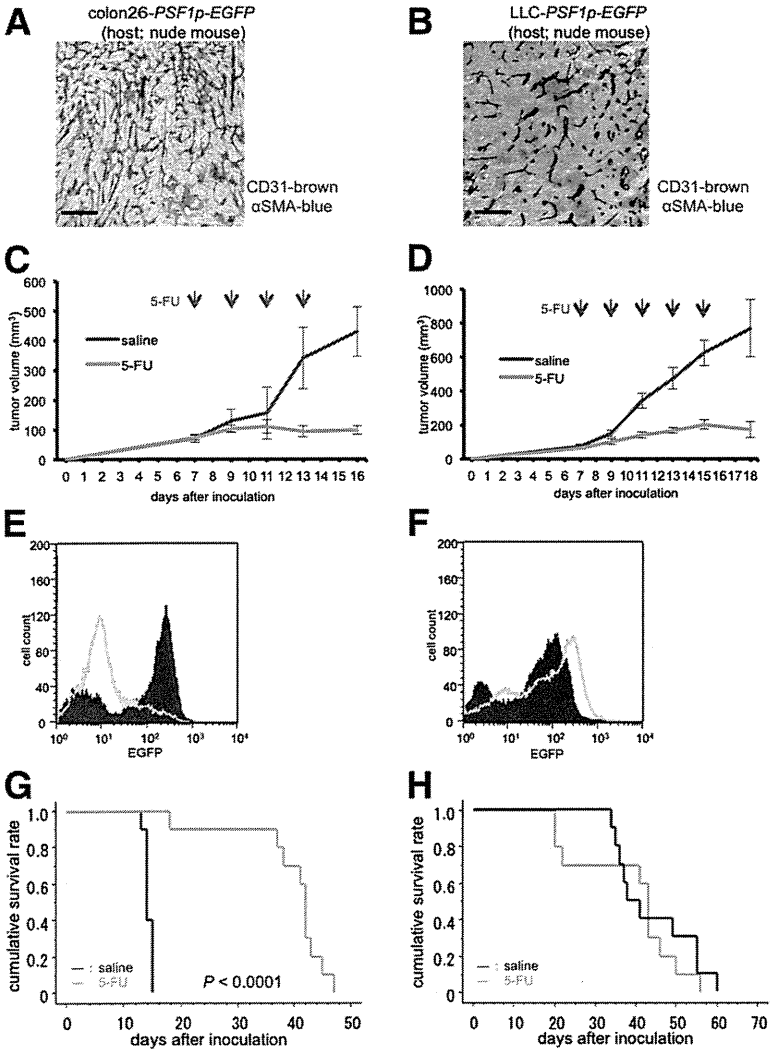

Figure 6 Relationship of maturation of blood vessels and survival of tumor-bearing mice after treatment with anticancer drug. **A** and **B**: Immunohistochemical staining of tumor sections derived from tumor inoculated by colon26- (**A**) and LLC- (**B**) *PSF1p-EGFP* cells into nude mice. Sections were stained with anti-CD31 antibody (brown) and anti—α-SMA antibody (blue). Scale bars: 200 μm. **C** and **D**: Time course of tumor volume after 5-FU administration *in vivo* using nude mice as in **A** or **B**, respectively. **Red arrows** indicate the date of 5-FU injection. **E** and **F**: Flow cytometric analysis of cells from tumor tissues on day 16 (as in **C**) or on day 18 (as in **D**), respectively. Data obtained by flow cytometry in the saline (control) group (**purple area**) and the 5-FU—injected group (**green line**) represent the results of multiple experiments. **G** and **H**: Kaplan-Meier curve of nude mice bearing colon26 tumors as in **C** or LLC tumors as in **D**, respectively, after 5-FU administration (n = 10 for each group).

tumor growth was inhibited, but inhibition of blood vessel maturation was not observed clearly in our studies.

As to other possible ways to inhibit the maturation of blood vessels in tumors, inhibition of the platelet-derived growth factor signal has been considered because of its effect on recruitment of mural cells near endothelial cells.[35] However, inhibition of the platelet-derived growth factor signal also decreased interstitial hypertension in tumor parenchyma for improvement of drug delivery,[36] suggesting that clear conclusions on inhibition of the maturation of blood vessels could not be drawn through the use of a platelet-derived growth factor inhibitor. Therefore, the specific molecular mechanism regulating the maturation of blood vessels, especially in LLC-type tumors, should be elucidated and used for inhibition of tumor blood vessel maturation.

Results of the present study suggest that cells composing the tumor microenvironment support the acquisition of drug resistance in CICs after cancer drug administration. How stromal cells in the tumor microenvironment change their characteristics to provide cancer cells with malignancy is completely unknown. We previously reported that exogenous molecular cues stimulate stromal cells to alter the cell fate of co-cultured hematopoietic stem cells.[37] When OP9 osteoblastic stromal cells were stimulated with epidermal growth factor or activated by transfection with the constitutive active form of erbB2 to exclude the direct effect of epidermal growth factor on hematopoietic stem cells, self-renewal of co-cultured hematopoietic stem cells was induced. On the other hand, when OP9 cells were stimulated with basic fibroblast growth factor, co-cultured hematopoietic stem cells quickly differentiated. Similarly, when endothelial cells were used as stromal cells and activated with the constitutive active form of AKT, self-renewal of co-cultured hematopoietic stem cells was induced.[38] On the other hand, when c-raf was transfected and the extracellular signal-regulated kinase pathway was activated in endothelial cells, differentiation of co-cultured hematopoietic stem cells was induced. Therefore, these findings suggest that different molecular cues that affect the same stromal cells alter behavior of the neighboring stem cell population via factors derived from stromal cells. In summary, niche cells of CICs/CSCs in the cancer microenvironment may intrinsically change their characteristics after cancer drug treatment or be affected indirectly by other cell components and may provide CICs/CSCs with acquisition of drug resistance. Further precise analysis will be necessary to investigate what kind of molecular mechanism underlies the induction of malignancy in CICs/CSCs.

Finally, we would like to emphasize that the tumor cell transplantation model reflects only a part of actual cancer tissue in patients. Tumor tissue in patients may comprise heterogeneous CICs/CSCs. Moreover, niche cells are not homogeneous. Therefore, the response to a cancer drug in the tumor environment varies even within the same patient. We need to clarify the central principle to support the malignant features of CICs/CSCs for the development of a new strategy to inhibit tumor growth.

Acknowledgments

We thank Keisho Fukuhara and Noriko Fujimoto for general assistance.

Supplemental Data

Supplemental material for this article can be found at *http://dx.doi.org/10.1016/j.ajpath.2013.01.019*.

References

1. Hanahan D, Weinberg RA: Hallmarks of cancer: the next generation. Cell 2011, 144:646–674
2. Gupta PB, Chaffer CL, Weinberg RA: Cancer stem cells: mirage or reality? Nat Med 2009, 15:1010–1012
3. Ben-Porath I, Thomson MW, Carey VJ, Ge R, Bell GW, Regev A, Weinberg RA: An embryonic stem cell-like gene expression signature in poorly differentiated aggressive human tumors. Nat Genet 2008, 40: 499–507
4. Wong DJ, Liu H, Ridky TW, Cassarino D, Segal E, Chang HY: Module map of stem cell genes guides creation of epithelial cancer stem cells. Cell Stem Cell 2008, 2:333–344
5. Somervaille TC, Matheny CJ, Spencer GJ, Iwasaki M, Rinn JL, Witten DM, Chang HY, Shurtleff SA, Downing JR, Cleary ML: Hierarchical maintenance of MLL myeloid leukemia stem cells employs a transcriptional program shared with embryonic rather than adult stem cells. Cell Stem Cell 2009, 4:129–140
6. Bao S, Wu Q, McLendon RE, Hao Y, Shi Q, Hjelmeland AB, Dewhirst MW, Bigner DD, Rich JN: Glioma stem cells promote radioresistance by preferential activation of the DNA damage response. Nature 2006, 444:756–760
7. Frank NY, Schatton T, Frank MH: The therapeutic promise of the cancer stem cell concept. J Clin Invest 2010, 120:41–50
8. Loebinger MR, Giangreco A, Groot KR, Prichard L, Allen K, Simpson C, Bazley L, Navani N, Tibrewal S, Davies D, Janes SM: Squamous cell cancers contain a side population of stem-like cells that are made chemosensitive by ABC transporter blockade. Br J Cancer 2008, 98:380–387
9. Miletti-González KE, Chen S, Muthukumaran N, Saglimbeni GN, Wu X, Yang J, Apolito K, Shih WJ, Hait WN, Rodríguez-Rodríguez L: The CD44 receptor interacts with P-glycoprotein to promote cell migration and invasion in cancer. Cancer Res 2005, 65: 6660–6667
10. Angelastro JM, Lamé MW: Overexpression of CD133 promotes drug resistance in C6 glioma cells. Mol Cancer Res 2010, 8:1105–1115
11. Cabarcas SM, Mathews LA, Farrar WL: The cancer stem cell niche—there goes the neighborhood? Int J Cancer 2011, 129:2315–2327
12. Kiel MJ, Morrison SJ: Maintaining hematopoietic stem cells in the vascular niche. Immunity 2006, 25:862–864
13. Mikkola HK, Orkin SH: The journey of developing hematopoietic stem cells. Development 2006, 133:3733–3744
14. Adams GB, Scadden DT: The hematopoietic stem cell in its place. Nat Immunol 2006, 7:333–337
15. Calabrese C, Poppleton H, Kocak M, Hogg TL, Fuller C, Hamner B, Oh EY, Gaber MW, Finklestein D, Allen M, Frank A, Bayazitov IT, Zakharenko SS, Gajjar A, Davidoff A, Gilbertson RJ: A perivascular niche for brain tumor stem cells. Cancer Cell 2007, 11:69–82
16. Nagahama Y, Ueno M, Miyamoto S, Morii E, Minami T, Mochizuki N, Saya H, Takakura N: PSF1, a DNA replication factor

expressed widely in stem and progenitor cells, drives tumorigenic and metastatic properties. Cancer Res 2010, 70:1215–1224
17. Beck B, Driessens G, Goossens S, Youssef KK, Kuchnio A, Caauwe A, Sotiropoulou PA, Loges S, Lapouge G, Candi A, Mascre G, Drogat B, Dekoninck S, Haigh JJ, Carmeliet P, Blanpain C: A vascular niche and a VEGF-Nrp1 loop regulate the initiation and stemness of skin tumours. Nature 2011, 478:399–403
18. Vermeulen L, De Sousa E, Melo F, van der Heijden M, Cameron K, de Jong JH, Borovski T, Tuynman JB, Todaro M, Merz C, Rodermond H, Sprick MR, Kemper K, Richel DJ, Stassi G, Medema JP: Wnt activity defines colon cancer stem cells and is regulated by the microenvironment. Nat Cell Biol 2010, 12:468–476
19. Takayama Y, Kamimura Y, Okawa M, Muramatsu S, Sugino A, Araki H: GINS, a novel multiprotein complex required for chromosomal DNA replication in budding yeast. Genes Dev 2003, 17: 1153–1165
20. Kamada K, Kubota Y, Arata T, Shindo Y, Hanaoka F: Structure of the human GINS complex and its assembly and functional interface in replication initiation. Nat Struct Mol Biol 2007, 14:388–396
21. Ueno M, Itoh M, Kong L, Sugihara K, Asano M, Takakura N: PSF1 is essential for early embryogenesis in mice. Mol Cell Biol 2005, 25: 10528–10532
22. Han Y, Ueno M, Nagahama Y, Takakura N: Identification and characterization of stem cell-specific transcription of PSF1 in spermatogenesis. Biochem Biophys Res Commun 2009, 380:609–613
23. Ueno M, Itoh M, Sugihara K, Asano M, Takakura N: Both alleles of PSF1 are required for maintenance of pool size of immature hematopoietic cells and acute bone marrow regeneration. Blood 2009, 113: 555–562
24. Takakura N, Watanabe T, Suenobu S, Yamada Y, Noda T, Ito Y, Satake M, Suda T: A role for hematopoietic stem cells in promoting angiogenesis. Cell 2000, 102:199–209
25. Takakura N, Huang XL, Naruse T, Hamaguchi I, Dumont DJ, Yancopoulos GD, Suda T: Critical role of the TIE2 endothelial cell receptor in the development of definitive hematopoiesis. Immunity 1998, 9:677–686
26. Wang R, Chadalavada K, Wilshire J, Kowalik U, Hovinga KE, Geber A, Fligelman B, Leversha M, Brennan C, Tabar V: Glioblastoma stem-like cells give rise to tumour endothelium. Nature 2010, 468:829–833
27. Ding L, Saunders TL, Enikolopov G, Morrison SJ: Endothelial and perivascular cells maintain haematopoietic stem cells. Nature 2012, 481:457–462
28. Bautch VL: Stem cells and the vasculature. Nat Med 2011, 17: 1437–1443
29. Conley SJ, Gheordunescu E, Kakarala P, Newman B, Korkaya H, Heath AN, Clouthier SG, Wicha MS: Antiangiogenic agents increase breast cancer stem cells via the generation of tumor hypoxia. Proc Natl Acad Sci U S A 2012, 109:2784–2789
30. Jain RK: Normalization of tumor vasculature: an emerging concept in antiangiogenic therapy. Science 2005, 307:58–62
31. Naito H, Takara K, Wakabayashi T, Kawahara H, Kidoya H, Takakura N: Changes in blood vessel maturation in the fibrous cap of the tumor rim. Cancer Sci 2012, 103:433–438
32. Ebos JM, Lee CR, Cruz-Munoz W, Bjarnason GA, Christensen JG, Kerbel RS: Accelerated metastasis after short-term treatment with a potent inhibitor of tumor angiogenesis. Cancer Cell 2009, 15: 232–239
33. Pàez-Ribes M, Allen E, Hudock J, Takeda T, Okuyama H, Viñals F, Inoue M, Bergers G, Hanahan D, Casanovas O: Antiangiogenic therapy elicits malignant progression of tumors to increased local invasion and distant metastasis. Cancer Cell 2009, 15:220–231
34. Kano MR, Bae Y, Iwata C, Morishita Y, Yashiro M, Oka M, Fujii T, Komuro A, Kiyono K, Kaminishi M, Hirakawa K, Ouchi Y, Nishiyama N, Kataoka K, Miyazono K: Improvement of cancer-targeting therapy, using nanocarriers for intractable solid tumors by inhibition of TGF-beta signaling. Proc Natl Acad Sci U S A 2007, 104: 3460–3465
35. Lindblom P, Gerhardt H, Liebner S, Abramsson A, Enge M, Hellstrom M, Backstrom G, Fredriksson S, Landegren U, Nystrom HC, Bergstrom G, Dejana E, Ostman A, Lindahl P, Betsholtz C: Endothelial PDGF-B retention is required for proper investment of pericytes in the microvessel wall. Genes Dev 2003, 17:1835–1840
36. Pietras K, Ostman A, Sjöquist M, Buchdunger E, Reed RK, Heldin CH, Rubin K: Inhibition of platelet-derived growth factor receptors reduces interstitial hypertension and increases transcapillary transport in tumors. Cancer Res 2001, 61:2929–2934
37. Takakura N, Kodama H, Nishikawa S, Nishikawa S: Preferential proliferation of murine colony-forming units in culture in a chemically defined condition with a macrophage colony-stimulating factor-negative stromal cell clone. J Exp Med 1996, 184:2301–2309
38. Kobayashi H, Butler JM, O'Donnell R, Kobayashi M, Ding BS, Bonner B, Chiu VK, Nolan DJ, Shido K, Benjamin L, Rafii S: Angiocrine factors from Akt-activated endothelial cells balance self-renewal and differentiation of haematopoietic stem cells. Nat Cell Biol 2010, 12:1046–1056

The American Journal of Pathology, Vol. 182, No. 5, May 2013

ELSEVIER

The American Journal of
PATHOLOGY

ajp.amjpathol.org

TUMORIGENESIS AND NEOPLASTIC PROGRESSION

Galectin-3 Accelerates M2 Macrophage Infiltration and Angiogenesis in Tumors

Weizhen Jia,* Hiroyasu Kidoya,* Daishi Yamakawa,* Hisamichi Naito,* and Nobuyuki Takakura*†

From the Department of Signal Transduction, Research Institute for Microbial Diseases, Osaka University, Osaka; and Japan Science and Technology Agency (JST),† K's Gobancho, Tokyo, Japan*

Accepted for publication January 10, 2013.

Address correspondence to Nobuyuki Takakura, M.D., Ph.D., Department of Signal Transduction, Research Institute for Microbial Diseases, Osaka University, 3-1 Yamadaoka, Suita, Osaka 565-0871, Japan. E-mail: ntakaku@biken.osaka-u.ac.jp.

It is widely accepted that robust invasion of tumor-associated macrophages resembling M2 macrophage correlates with disease aggressiveness by affecting cancer cell invasion, metastasis, and angiogenesis. Many chemokines that induce migration of macrophages have been identified during inflammatory responses; however, further precise analysis of macrophage migration in the tumor microenvironment is required. Here, we analyzed the function of galectin-3 (Gal-3; gene *LGALS3*, alias *Gal3*) for macrophage chemotaxis using *Gal3*$^{-/-}$ mice as hosts, and a tumor allograft model. We engineered a concentration gradient of Gal-3 produced by the tumor. In this model, we found that macrophage infiltration was enhanced in tumors developing in these *Gal3*$^{-/-}$ mice relative to the *Gal3*$^{+/+}$ animals. This was accompanied by enhanced tumor angiogenesis and tumor growth in *Gal3*$^{-/-}$ mice. We found that macrophages of the M2 phenotype were dominant in infiltrates in the *Gal3*$^{-/-}$ mice and that they expressed only low levels of Gal-3. *Gal3* knockdown by siRNA in macrophages resulted in enhanced chemotaxis. These data suggest that M2-like macrophages migrate into the tumor along a Gal-3 gradient and that high-level Gal-3 expression in the tumor results in acceleration of angiogenesis and tumor growth. Therefore, Gal-3 could be a potential target for the development of new treatments to inhibit tumor growth. *(Am J Pathol 2013, 182: 1821–1831; http://dx.doi.org/10.1016/j.ajpath.2013.01.017)*

Neovascularization is an indispensable event for tissue/organ development. New blood vessel formation observed under pathologic and physiological conditions occurs mainly by sprouting angiogenesis (ie, the development of a new branch from pre-existing vessels).[1] In sprouting angiogenesis, proangiogenic factors released from hypoxic regions or sites of inflammation directly induce migration and proliferation of endothelial cells (ECs). Moreover, nonvascular cells infiltrating into the region produce angiogenic factors that induce angiogenesis indirectly.[2,3]

We previously reported that hematopoietic stem/progenitor cells and CD11b^{low} immature myeloid cells/monocytes induce angiogenesis and maturation of newly developed blood vessels by secretion of angiopoietin-1, a ligand for receptor tyrosine kinase Tie2 expressed on ECs.[4,5] In addition, it is widely accepted that matrix metalloproteinase derived from mast cells, neutrophils, and macrophages promotes angiogenesis by matrix remodeling, and that vascular endothelial growth factor secreted by these cell populations also regulates angiogenesis.[6] Among hematopoietic lineages, the relationships of macrophages to angiogenesis have been examined extensively and crucial roles, especially of tumor-associated macrophages and Tie2-expressing macrophages, for tumor angiogenesis have been reported.[7,8]

Monocyte chemoattractant protein-1 (also known as chemokine ligand 2) and colony-stimulating factor-1 (also known as macrophage-colony-stimulating factor) are well-known chemoattractants for monocytes/macrophages, but other factors such as placental growth factor, chemokine ligand 3 (macrophage inflammatory protein 1), chemokine ligand 4, chemokine ligand 5 (regulated on activation normal T-cell expressed and secreted), and vascular endothelial growth factor also have been reported to act this way.[9,10] Therefore, further precise investigation is required to identify the molecules inducing monocyte/macrophage migration.

Here, we investigated relationships among galactose-binding lectin-3 (alias galectin-3; Gal-3), monocytes/macrophages, and

Supported by a Grant-in-Aid for Scientific Research from the Ministry of Education, Culture, Sports, Science, and Technology and the Japan Society for the Promotion of Science.

http://dx.doi.org/10.1016/j.ajpath.2013.01.017

angiogenesis. Galectins are a family of lectins containing conserved carbohydrate-recognition domains specific for β-galactoside.[11] Gal-3 is a 32-kDa protein containing one carbohydrate-recognition domain and an N-terminal nonlectin domain. Different functions for Gal-3 in development, immune reactions, and tumorigenesis have been reported.[12] In macrophages, expression of Mac-2 (another name for Gal-3) has been reported. Published evidence suggests that Gal-3 may influence the migration of monocytes/macrophages.[13] However, the precise function of Gal-3 for monocyte/macrophage migration in the context of angiogenesis has not been clarified.

Thus far, although it has been reported that the mobility of ECs is enhanced by scaffolding generated through the binding of Gal-3 to integrin, *in vivo* roles of Gal-3 in angiogenesis have been minimally investigated. Because it has been reported that tumor cells express abundant Gal-3[12,14] and tumor angiogenesis is one available model for investigating Gal-3 function, we examined the role of Gal-3 in angiogenesis using *Gal3*-deficient mice.

Materials and Methods

Animals

C57BL/6 mice (7 to 8 weeks of age) were purchased from Japan SLC (Shizuoka, Japan). *Gal3* knockout (KO) mice (7 to 8 weeks of age) were generated as previously described.[15] Animals were housed in environmentally controlled rooms of the animal experimentation facility at Osaka University. All experiments were performed in accordance with the guidelines of Osaka University Committee for Animal and Recombinant DNA Experiments. Mice were handled and maintained according to Osaka University guidelines for animal experimentation.

Cell Culture

Cell lines, including B16 (mouse melanoma), mouse Lewis lung carcinoma (LLC), and J774 (murine macrophage), were purchased from the Riken cell bank (Tsukuba, Japan). The B16 and LLC cell lines were cultured in Dulbecco's modified Eagle's medium (Sigma, St. Louis, MO) supplemented with 10% fetal bovine serum and 1% penicillin/streptomycin. The J774 cell line was cultured in Dulbecco's modified Eagle's medium supplemented with 10% fetal bovine serum, 1% penicillin/streptomycin, and 2 mol/L L-glutamine (Gibco, Life Technologies, St. Paul, Brazil). Single-cell suspensions from tumor tissue were produced as previously described.[16] Murine bone marrow–derived macrophages ($CD45^{high}$ $CD11b^{high}$ $F4/80^{high}$) were isolated and prepared as previously described[16] and were cultured in RPMI-1640 (Sigma) supplemented with 10% fetal bovine serum, 1% penicillin/streptomycin, 2 mmol/L L-glutamine, and 50-ng/mL murine M-colony-stimulating factor (PeproTech, Rocky Hill, NJ). These bone marrow–derived macrophages were maintained for 7 days in a CO_2 incubator.

Quantitative Real-Time RT-PCR

Total RNA was extracted from cells and tumor tissues using RNeasy-plus mini kits (Qiagen, Hilden, Germany) and was reverse-transcribed using the PrimeScript RT reagent Kit (Takara, Kyoto, Japan) according to the manufacturer's protocol. Real-time PCR analysis was performed using Platinum SYBR Green qPCR SuperMix-UDC (Invitrogen, Carlsbad, CA) and an Mx3000p QPCR System (Stratagene, La Jolla, CA). The baseline and threshold were adjusted according to the manufacturer's instructions. The level of the target gene expression was normalized to that of glyceraldehyde-3-phosphate dehydrogenase in each sample. We used the following primer sets for mouse genes: 5′-CCACGTCGTAGCAAACCACCA-3′ (forward) and 5′-AGGAGCACGTAGTCGGGGCA-3′ (reverse) for tumor necrosis factor-α, 5′-TCCTCTCTGCAAGAGACTTCC-ATCC-3′ (forward) and 5′-GGGAAGGCCGTGGTTGT-CACC-3′ (reverse) for *IL6*, 5′-AGGCTCATCCAGAG-CCCGGAG-3′ (forward) and 5′-AGGGTGGTGCGGCTG-GACTT-3′ (reverse) for inducible nitric oxide synthase, 5′-TCGGTGGACTGTGGACGAGCA-3′ (forward) and 5′-TCCCGCCTTTCGTCCTGGCA-3′ (reverse) for macrophage mannose receptor 1 (MRC1), 5′-CCCCAGGCAGAGAA-GCATGGC-3′ (forward) and 5′-GGGGAGAAATCGATG-ACAGCGCC-3′ (reverse) for *IL10*, 5′-TCAGCCAGATG-CAGTTAACGCCC-3′ (forward) and 5′-GCTTCTTTGGG-ACACCTGCTGCT-3′ (reverse) for monocyte chemoattractant protein-1, 5′-TGCCCTATGACCTGCCCTT-3′ (forward) and 5′-TCCTGCTTCGTGTTACACACAA-3′ (reverse) for *Gal3* and, finally, 5′-TGGCAAAGTGGAGATTGTTGCC-3′ (forward) and 5′-AAGATGGTGATGGGCTTCCCG-3′ (reverse) for glyceraldehyde-3-phosphate dehydrogenase (*Gapdh*).

Western Blotting Analysis

Methods for Western blotting were as previously described.[17] Briefly, lysates from whole cells were resolved in SDS-PAGE. Proteins electrophoretically separated using 12.5% SDS-PAGE gels were transferred to nylon membranes (Amersham, Buckinghamshire, UK) by a wet blotting procedure and incubated with the following antibodies: rat anti-mouse Gal-3/MAC-2 (Cedarlane, Ontario, Canada); and anti-mouse glyceraldehyde-3-phosphate dehydrogenase (Millipore, Temecula, CA). Proteins were detected with horseradish-peroxidase–conjugated goat anti-rat IgG, goat anti-mouse IgG (Jackson Laboratories, Bar Harbor, ME) secondary antibodies and ECL reagents (Amersham). The blots were scanned with an imaging densitometer LAS-3000 mini (Fujifilm, Tokyo, Japan).

RNA Interference

siRNA specific to mouse Gal-3 and negative control siRNA were purchased from Sigma and transfected into J774 cells using Lipofectamine 2000 (Invitrogen) according to the

manufacturer's instructions. The effect of siRNA on Gal-3 expression was observed using Western blotting with an anti–Gal-3/MAC-2 antibody (Cedarlane) and real-time PCR.

Migration Analysis

Migration analysis was performed using 5-μm pore-size cell culture inserts in 24-well plates (Corning, Chelmsford, UK). J774 cells or bone marrow–derived macrophages (1×10^4) were seeded into the top of the Transwell chambers precoated with fibronectin (Corning, Tokyo, Japan), and 8 μg/mL recombinant Gal-3 (R&D Systems, Minneapolis, MN) was added into the lower well. After 8 hours of incubation, cells on the upper membrane surface were removed with a cotton swab. Cells on the lower membrane surface were fixed with 4% formaldehyde and stained with Mounting Medium with DAPI (Vector Laboratories, Burlingame, CA).

In Vivo Tumor Cell Allograft Model

B16 or LLC tumor cells (1×10^6 per mouse in 0.1 mL PBS) were inoculated subcutaneously into wild-type C57BL/6 or *Gal3* KO mice (7 to 8 weeks of age). Tumors were dissected 18 days after implantation (in allografts using bone marrow–transplanted chimeric mice, discussed later (see *Bone Marrow Transplantation*)). Tumor volumes were measured with calipers every 3 days and were calculated as follows: width × width × length × 0.52.[18]

Immunohistochemistry

Immunostaining analysis was performed on 10-μm cryostat sections of mouse tumor tissue. Procedures for tissue fixation and staining of sections with antibodies were as described previously.[4] For immunohistochemistry, rat anti-mouse F4/80 antibody (AbD Serotec, Raleigh, NC), rat anti-mouse CD206 (MRC1) antibody (AbD Serotec), rat anti-mouse CD31 antibody (BD Pharmingen, San Jose, CA), and hamster anti-mouse CD31 antibody (Millipore) were used for staining and anti-rat IgG Alexa Fluor 488 (Invitrogen), anti-rat IgG Alexa Fluor 546 (Invitrogen), and anti-Armenian hamster FITC (eBioscience, San Diego, CA) as the secondary antibodies. Cell nuclei were visualized with TO-PRO-3 (Invitrogen). To measure hypoxia in tumor tissues, 60 mg/kg HypoxyProbe-1 (Hypoxyprobe, Inc, Burlington, MA) was injected intraperitoneally 1 hour before sacrificing the mice. Tumor sections were stained using an anti-HypoxyProbe antibody. Sections were observed by conventional microscopy (brightfield) (DM5500 B; Leica, Wetzlar, Germany) or confocal microscopy (TCS/SP5; Leica), and images were acquired with a digital camera (DFC500; Leica). In all analyses, an isotype-matched control Ig was used as a negative control and it was confirmed that the positive signals were not derived from a nonspecific background. Images were processed using Photoshop CS2 software version 9.0.2 (Adobe Systems, San Jose, CA). All images shown are representative of six or more independent experiments.

Flow Cytometry

Flow cytometric analysis was performed as described previously.[5] Fluorescence-labeled anti-mouse antibodies specific for F4/80, CD206 (MRC1) (AbD Serotec), CD11b, and CD45 (BD Pharmingen) were used. Stained cells were analyzed with a FACSCalibur or FACSAria (BD Biosciences) using FlowJo software version 7.6.1 (TreeStar, Ashland, OR) and sorted by a FACSAria. Dead cells were excluded by propidium iodide staining or analyses using the two-dimensional profile of the forward versus side scatter.

Bone Marrow Transplantation

Bone marrow cells from wild-type mice were transplanted into wild-type C57BL/6 or *Gal3* KO mice (7 to 8 weeks of age). Bone marrow cells were obtained by flushing the tibias and femurs of age-matched donor wild-type C57BL/6 mice. Bone marrow transplantation (BM-T) was performed using lethally irradiated (10.0 Gy) wild-type C57BL/6 or *Gal3* KO mice by intravenous infusion of 1×10^6 donor whole bone marrow cells. Four weeks after transplantation, BM chimeric mice received an inoculation of B16 or LLC tumor cells (1×10^6 per mouse in 0.1 mL PBS) subcutaneously, and tumor tissues were dissected 18 days after implantation. Tumor volumes were measured with calipers every 3 days and calculated as follows: width × width × length × 0.52.[18]

Statistical Analysis

All data are presented as means ± SD. Statistical analysis was performed by the Tukey-Kramer multiple comparison test using the statcel version 2 software package (OMS, Saitama, Japan). When only two groups were compared, a two-sided Student's *t*-test was used. A P value less than 0.05 was considered statistically significant.

Results

Tumor Growth Is Enhanced in *Gal3*$^{-/-}$ Mice

It has been suggested that Gal-3 induces angiogenesis by directly promoting chemotaxis of ECs.[19] Functional chemotaxis also may involve other cell types, such as monocytes/macrophages, because of the known function of Gal-3 in macrophage migration.[13,20] Macrophages act as proangiogenic accessory cell components in tumors by secreting several angiogenic factors such as vascular endothelial growth factor, matrix metalloproteinases, and others.[21–23] Therefore, it was hypothesized that Gal-3 in the tumor environment accelerates tumor angiogenesis via macrophage chemotaxis, resulting in tumor growth. To test this, *Gal3* mutant (*Gal3*$^{-/-}$) mice were used as tumor-bearing hosts because macrophages themselves

produce Gal-3 and chemotaxis caused by tumor-derived Gal-3 would not be assessable. Although Gal-3 production from tumor stromal cells is absent in *Gal3*$^{-/-}$ mice, tumor cell–derived Gal-3 should generate a concentration gradient from the tumor, enabling visualization of *Gal3*-deficient macrophage infiltration into tumor tissue.

We used two cancer cell lines, B16 mouse melanoma and LLC mouse lung cancer cells for the allograft model. We inoculated these cells into *Gal3*$^{+/+}$ (wild-type) and *Gal3*$^{-/-}$ mice and evaluated tumor growth. These results showed enhancement of tumor growth in *Gal3*$^{-/-}$ mice compared with *Gal3*$^{+/+}$ mice in both B16 (Figure 1, A–C) and LLC tumors (Figure 1, D–F).

Macrophage Migration Is Induced by Gal-3

Both B16 and LLC tumor tissues were found to express Gal-3 more strongly than normal cells such as those from skin, spleen (B cells), liver, and lung, both at the mRNA (Figure 1G) and protein levels (Figure 1H). This suggests that cancer cell–derived Gal-3 does form a concentration gradient in *Gal3*$^{-/-}$ mice and may induce migration of monocytes/macrophages into tumors. The number of infiltrated F4/80-positive macrophage lineage cells was significantly higher in tumors that developed in *Gal3*$^{-/-}$ mice than in *Gal3*$^{+/+}$ mice (Figure 2, A and B).

Next, we investigated if exogenous Gal-3 induces chemotaxis of macrophages and if endogenous Gal-3 in macrophages would obscure this chemotaxis. We used J774, a macrophage cell line, and silenced Gal-3 expression by siRNA (Figure 2C). As expected, knockdown of endogenous Gal-3 enhanced transmigration of J774 macrophages (Figure 2, D and E).

We next isolated CD45^{high} CD11b^{high} F4/80^{high} macrophages from the bone marrow of *Gal3*$^{+/+}$ or *Gal3*$^{-/-}$ mice and confirmed a lack of Gal-3 in those from *Gal3* KO animals (Figure 2F). By using these primary macrophages, we observed chemotaxis stimulated by Gal-3. As was seen in the J774 cell line, a lack of endogenous Gal-3 resulted in enhanced macrophage chemotaxis along a Gal-3 gradient (Figure 2, G and H).

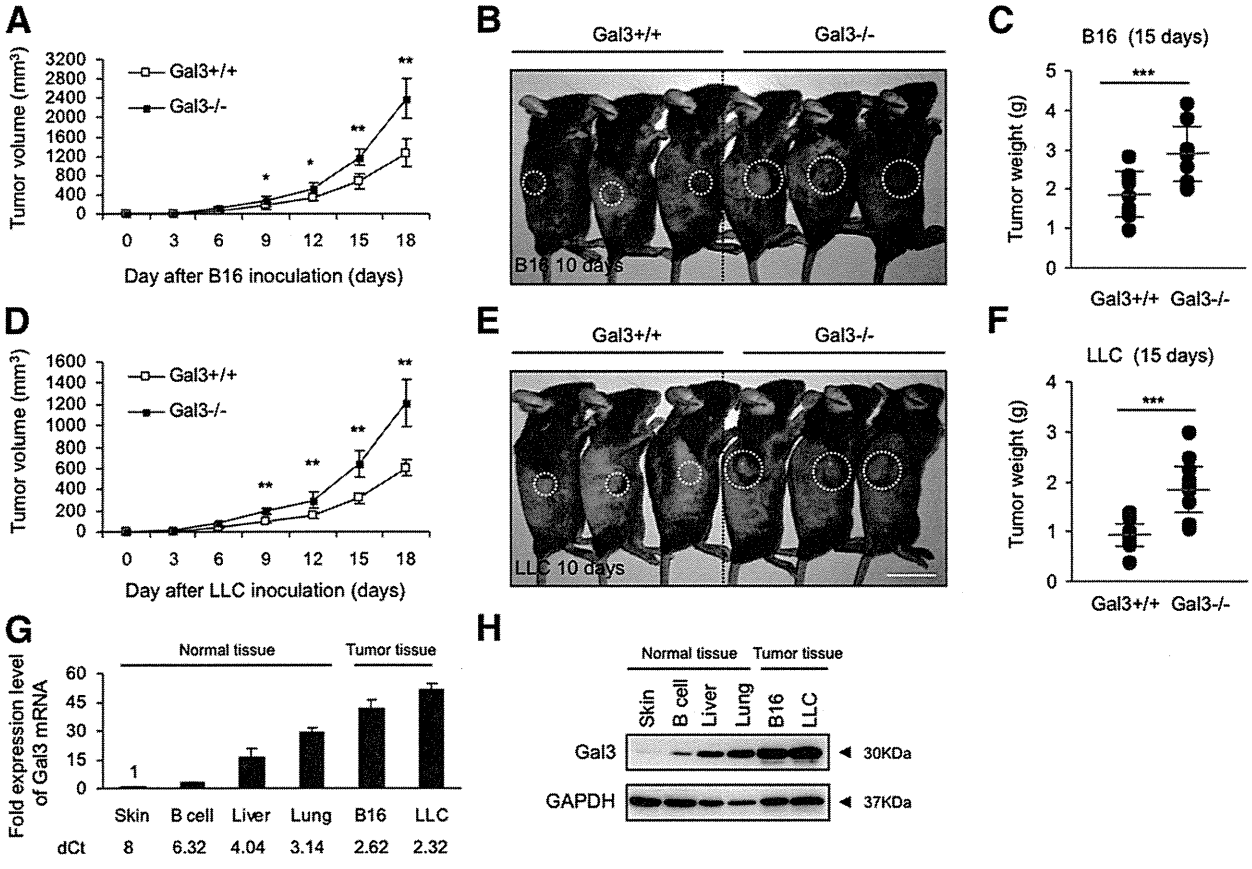

Figure 1 Tumor growth *Gal3*$^{-/-}$ mice. **A:** Tumor growth curves of B16 (melanoma) cells on s.c. injection into *Gal3*$^{+/+}$ (wild-type) or *Gal3*$^{-/-}$ (KO) mice ($n = 10$ for each group). Data are means ± SEM. $^{*}P < 0.05$, $^{**}P < 0.01$. **B:** Gross appearance of tumors derived from B16 cells on day 10 after tumor cell inoculation. **Dashed lines** indicate tumor area. Scale bar = 2 cm. **C:** Tumor weight on day 15 after B16 cell inoculation ($n = 10$). Data are means ± SEM. $^{***}P < 0.001$. **D:** Tumor growth curves of LLC cells on s.c. injection into *Gal3*$^{+/+}$ or *Gal3*$^{-/-}$ mice ($n = 10$ for each group). Data are means ± SEM. $^{**}P < 0.01$. **E:** Gross appearance of tumors derived from LLC cells on day 10 after tumor cell inoculation. **Dashed lines** indicate tumor area. Scale bar = 2 cm. **F:** Tumor weight on day 15 after LLC cell inoculation ($n = 10$). Data are means ± SEM. $^{***}P < 0.001$. **G:** Quantitative real-time PCR analysis of Gal-3 mRNA expression in tumor (B16, LLC) and normal tissue-derived single-cell suspensions (total skin, liver, lung, or B cell from spleen). Threshold values for target genes normalized against the level of glyceraldehyde-3-phosphate dehydrogenase (GAPDH) **ΔCT** values (dCT) are shown under the graph ($n = 3$). **H:** Western blot analysis of Gal-3 expression in whole-cell extracts of tumor (B16, LLC) and normal tissue-derived single-cell suspensions (total skin, liver, lung, or B cell from spleen) with anti–Gal-3/Mac2 and anti-GAPDH antibodies.

M2 Macrophage Infiltration Is Enhanced in Tumors Developing in *Gal3*$^{-/-}$ Mice

Because we found abundant F4/80-positive macrophage lineage cells migrating into tumors developing in *Gal3*$^{-/-}$ mice, we identified their subtype. We confirmed that a population of CD11b^{high} F4/80^{high} macrophages was more highly abundant in both B16 and LLC tumors developing in *Gal3*$^{-/-}$ mice than in *Gal3*$^{+/+}$ mice (Figure 3A). Macrophages in tumors from *Gal3*$^{-/-}$ mice expressed MRC1 (CD206), an M2 macrophage marker, more strongly than in *Gal3*$^{+/+}$ mice (Figure 3B). Moreover, they expressed IL10 and monocyte chemoattractant protein-1 strongly as well as MRC1 at the mRNA level, a characteristic M2 macrophage gene signature (Figure 3C).[24] LLC but not B16 tumors in *Gal3*$^{+/+}$ mice expressed tumor necrosis factor-α more abundantly than in *Gal3*$^{-/-}$ mice. M2 macrophages were more abundant in LLC than B16 tumors. Therefore, M1 macrophage-mediated effects may be more apparent in LLC tumors of *Gal3*$^{+/+}$ mice.

The earlier-described data suggest that cells similar to M2 macrophages may migrate selectively into the tumor parenchyma when Gal-3 production is higher in the tumor than in nontumor tissue, such that a concentration gradient occurs. Moreover, it was possible that Gal-3 expression in M2 macrophages was constitutively lower and they more easily migrated into Gal-3-producing areas. We therefore divided bone marrow CD11b^{high} F4/80^{high} macrophages into two fractions, that is, MRC1^{low} and MRC1^{high} (Figure 3D), and quantified their Gal-3 expression (Figure 3E). MRC1 mRNA expression correlated with the protein level in macrophages. As expected, Gal-3 mRNA expression was lower in MRC1^{high} than in MRC1^{low} macrophages.

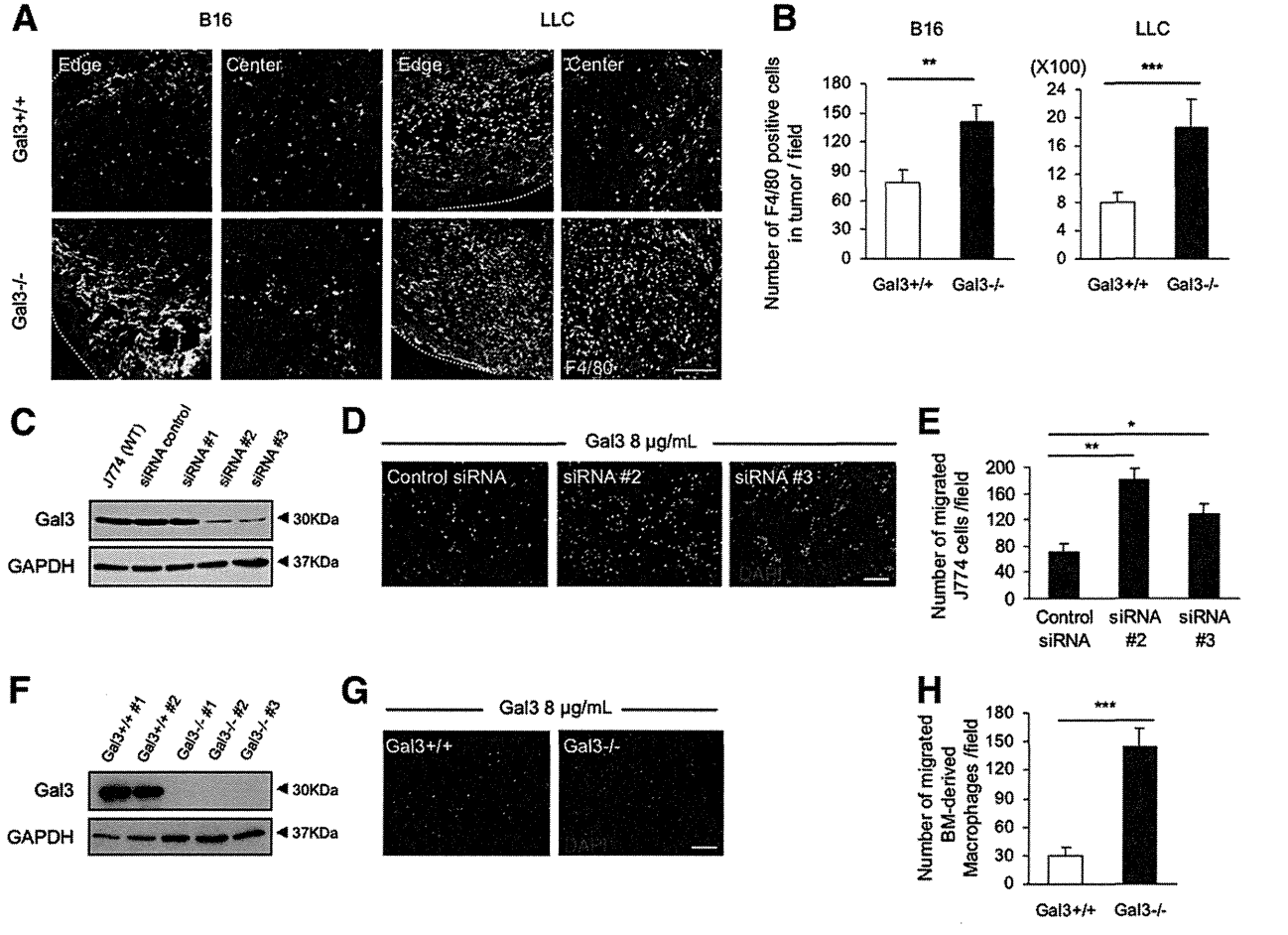

Figure 2 Migration of macrophages stimulated by Gal-3. **A:** Immunofluorescence staining of F4/80 (green) and TO-PRO-3 (blue) in the B16 or LLC tumor sections from *Gal3*$^{+/+}$ or *Gal3*$^{-/-}$ mice. Scale bar = 200 μm. **B:** Quantitative evaluation of migrated F4/80-positive macrophages in B16 or LLC tumors. Data are means ± SEM. $^{**}P < 0.01$, $^{***}P < 0.001$ (five random fields of 10 independent tumor sections). **C:** Western blot analysis of Gal-3 expression in J774 cells after silencing by RNA interference. Three different Gal-3-specific siRNAs (siRNA#1, siRNA#2, and siRNA#3) and control siRNA were used. **D:** Migration analysis using the Transwell technique. Representative images of migrated J774 cells stained with DAPI. Scale bar = 200 μm. **E:** Quantification of migrated J774 cells from five random fields of four independent samples. Data are means ± SEM. $^{*}P < 0.05$, $^{**}P < 0.01$. **F:** Western blot analysis of Gal-3 expression in bone marrow–derived macrophages (CD45^{high} CD11b^{high} F4/80^{high}) from *Gal3*$^{+/+}$ or *Gal3*$^{-/-}$ mice. Numbers 1, 2, and 3 are different individual mice. **G:** Migration analysis using bone marrow–derived macrophages as in **F**. Representative images of migrated cells stained with DAPI are shown. Scale bar = 200 μm. **H:** Quantification of migrated bone marrow–derived macrophages from five random fields of four independent samples. Data are means ± SEM. $^{***}P < 0.001$. GAPDH, glyceraldehyde-3-phosphate dehydrogenase.

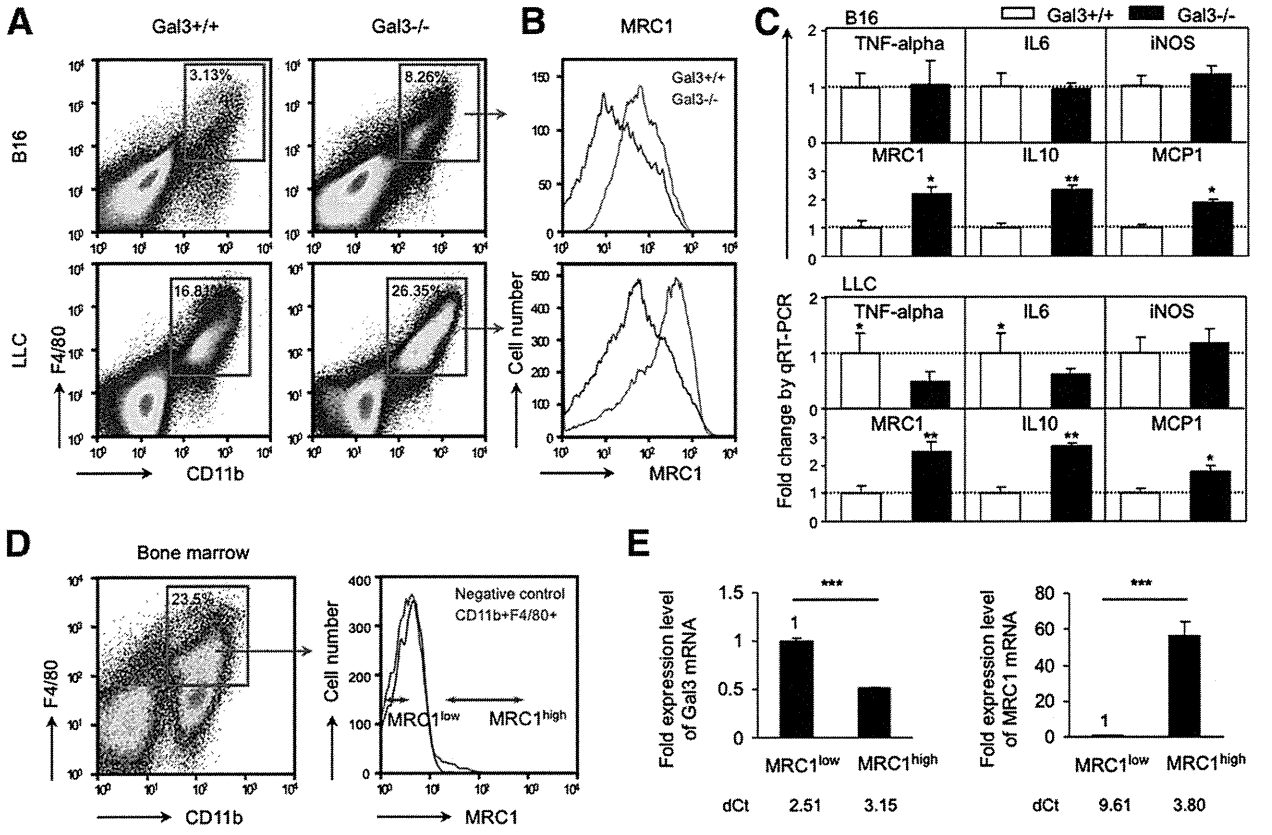

Figure 3 Increased M2 macrophage migration in *Gal3*$^{-/-}$ mice. **A:** Flow cytometric analysis of CD11b^{high} F4/80^{high} macrophages in B16 or LLC tumors in *Gal3*$^{+/+}$ or *Gal3*$^{-/-}$ mice. The population of CD11b^{high} F4/80^{high} macrophages within total cells in the tumor is shown in the gated **red box. B:** Histogram showing MRC1 expression intensity in the CD11b^{high} F4/80^{high} macrophages gated by the **red box** in **A.** Flow cytometric analysis was performed on day 12 after tumor cell implantation. Data are representative of B16 (n = 18) or LLC (n = 24) tumors. **C:** Quantitative real-time PCR analysis of mRNA expression in CD45^{high} CD11b^{high} F4/80^{high}-expressing tumor macrophages in B16 or LLC tumors in *Gal3*$^{+/+}$ or *Gal3*$^{-/-}$ mice. Data are means ± SEM. $^{*}P < 0.05$, $^{**}P < 0.01$ (n = 5). **D** and **E:** Analysis of Gal-3 expression in bone marrow–derived MRC1^{low} and MRC1^{high} macrophages from WT mice. **D:** Representative flow cytometric plots of cells from bone marrow of WT mice. **Left:** CD11b^{high} F4/80^{high} macrophage fraction is gated by the **red box** (23.5% ± 2.58%). **Right:** Histogram showing MRC1 expression intensity in CD11b^{high} F4/80^{high} macrophages. MRC1^{low} and MRC1^{high} macrophages were sorted as indicated (**right**). **E:** Quantitative real-time PCR analysis of Gal-3 and MRC1 mRNA expression in MRC1^{low} and MRC1^{high} macrophages sorted as in **C.** Threshold values for target genes normalized against the level of glyceraldehyde-3-phosphate dehydrogenase (**ΔCT** values; dCt) are shown under the graph. Data are means ± SEM. $^{***}P < 0.001$ (n = 4). iNOS, inducible nitric oxide synthase; MCP1, monocyte chemoattractant protein-1; TNF, tumor necrosis factor.

Tumor Angiogenesis Is Enhanced in Tumors Developing in *Gal3*$^{-/-}$ Mice

It is widely accepted that M2 macrophages promote angiogenesis.[25,26] Therefore, enhanced tumor growth in *Gal3*$^{-/-}$ is suggested to be induced by increased angiogenesis as a result of infiltration by M2-like macrophages. Hence, we investigated the localization of MRC1-positive macrophages in the tumor microenvironment. As shown in Figure 4, A–C, higher numbers of MRC-positive macrophages were observed in both B16 and LLC tumors developing in *Gal3*$^{-/-}$ than in *Gal3*$^{+/+}$ mice. Moreover, co-localization of MRC1-positive cells with CD31-positive ECs indicated that more of these cells were interacting with blood vessels in both B16 and LLC tumors in *Gal3*$^{-/-}$ mice.

The number of blood vessels identified as CD31^{+} was significantly higher in both B16 and LLC tumors developing in *Gal3*$^{-/-}$ than in *Gal3*$^{+/+}$ mice (Figure 4, D and E). It is possible that a mere increase in the number of blood vessels does not necessarily correlate with effective blood circulation in tumors and that nonfunctional blood vessel formation increases severe hypoxia.[27] We therefore evaluated hypoxic conditions and found that hypoxia was not more severe in tumors developing in *Gal3*$^{-/-}$ mice (Figure 4, F and G), suggesting that functional blood vessels are induced in tumors in *Gal3*$^{-/-}$ mice, enhancing tumor growth.

Restoration of Gal-3 in Bone Marrow Cells of *Gal3*$^{-/-}$ Mice Abrogates Enhanced Tumor Growth

Lack of Gal-3 in bone marrow macrophage lineage cells may be responsible for the enhancement of M2-like macrophage infiltration into tumors, resulting in induction of tumor angiogenesis and enhanced tumor growth. To test this hypothesis, we replaced the bone marrow of *Gal3*$^{-/-}$ mice with cells from *Gal3*$^{+/+}$ mice by BM-T and analyzed tumor growth and angiogenesis using these chimeric mice [*Gal3*$^{-/-}$ (BM-T)